



Coulomb Effects on the Spin Polarization in Quantum Wires

Anton Heiðar Þórólfsson



**Faculty of Physical Sciences
University of Iceland
2012**

Coulomb Effects on the Spin Polarization in Quantum Wires

Anton Heiðar Þórólfsson

60 ECTS thesis submitted in partial fulfillment of a
Magister Scientiarum degree in Physics

Advisors
Andrei Manolescu
Viðar Guðmundsson

Faculty Representative
Viðar Guðmundsson

Faculty of Physical Sciences
School of Engineering and Natural Sciences
University of Iceland

Reykjavik, 30 August 2012

Coulomb Effects on the Spin Polarization in Quantum Wires

60 ECTS thesis submitted in partial fulfillment of a *Magister Scientiarum* degree in physics

Copyright © 2012 Anton Heiðar Þórólfsson
All rights reserved

Faculty of Physical Sciences
School of Engineering and Natural Sciences
University of Iceland
VRIL, Hjarðarhagi 2-6
107 Reykjavík
Iceland

Telephone: 525 4700

Bibliographic information:

Anton Heiðar Þórólfsson, 2012, *Coulomb Effects on the Spin Polarization of Quantum Wires*, Master's thesis, Faculty of Physical Sciences, University of Iceland, pp. 52.

ISBN XX

Printing: Prentsmiðja Háskólaprent ehf.
Reykjavík, Iceland, 30 August 2012

Abstract

We study a two-dimensional electron gas in a long, continuous nanowire with lateral confinement, in an external magnetic field. Three different materials are considered, GaAs, InAs and InSb. We take into account Rashba and Dresselhaus spin-orbit interactions and the Coulomb interaction within the Hartree-Fock approximation. The energy spectra, charge, and spin densities, together with charge and spin currents are calculated and compared, with and without the Coulomb interaction in a variable magnetic field. We show that the spin currents may be amplified by the Coulomb interaction.

Acknowledgements

First of all I thank my advisor Andrei Manolescu who let me into his MSc program. He has taught me a lot for the past two years and he's always happy to help and explain to me whatever I couldn't understand with remarkable patience. I thank Viðar Guðmundsson, my advisor as well, for his support and helpfulness at every turn.

Other students of Andrei and Viðar who started before me were always glad to help me. Help with programming and other computer issues they had to deal with themselves when they began their studies. Specially I thank Csaba Daday, Gunnar Þorgilsson and Kristinn Torfason. Without their help starting this program would have been an ordeal. I thank Sigurður Ingi Erlingsson for answering my questions and lending me literature while Andrei was abroad. I thank Catalina and Anna for reviewing my thesis and giving me good notes to make it better.

I thank my family for supporting me through all of this. They always come through for me and I know they always will. Finally I thank my friends for moral support through tough times.

Contents

1	Introduction	1
1.1	Background	1
1.2	Fabrication of Quantum Systems	1
2	Description of the System	3
2.1	Quantum Wire	3
2.2	Hamiltonian of a Quantum Wire	4
2.2.1	The Basis States with Hard Walls	4
2.2.2	Soft Confinement	5
2.2.3	Chemical Potential	5
2.2.4	Magnetic field	7
2.2.5	Zeeman term	7
3	Spin-Orbit Interaction	8
4	Charge and Spin Densities	10
4.1	Operators and Expected Values	10
4.2	SOI Effects on the Spin Polarization	11
5	Charge and Spin Currents	15
5.1	Current Density Operators	15
5.2	Expectation Value of Current Densities	15
6	Coulomb Interaction	21
6.1	Hartree-Fock	21
6.2	Effects of Coulomb Interactions on Energy Spectra, Densities and Currents	23
7	Spin and Current Densities for Variable Magnetic Fields	28
7.1	Magnetic Field in z Direction and Symmetric Confinement . .	28
7.2	Magnetic Field in z Direction and Asymmetric Confinement .	34
7.3	Magnetic Field in y Direction	39

8	Summary and Conclusions	42
A	Clarification of some Calculations	44
A.1	Function to calculate matrix elements of magnetic part	44
A.2	Orbital Contribution to Current Densities	45
A.3	SOI Contribution to Current Densities	46
A.4	Exchange Contribution to Current Densities	46
A.5	Prefactors and Units for Current Densities	48
	Bibliography	49

Chapter 1

Introduction

1.1 Background

Spintronics of semiconductors is a fascinating field revealing more real life applications every day. For the last few decades, the processing powers of computers has increased exponentially by decreasing the size of transistor in processing chips. While the electronics become smaller, the effects of quantum mechanics become more visible and research in these fields become more important. In this thesis a continuous quantum wire in an external magnetic field is investigated and interesting effects analyzed more closely. Three different binary compounds are studied. Gallium arsenide (GaAs), indium arsenide (InAs) and indium antimonide (InSb). These are so called III-V semiconductors, named so since their elements are from periods III to V in the periodic table of elements. The crystals of those compounds have a zinc blende structure where each atom has four nearest neighbors of the other type and the form of a regular tetrahedron[5]. In this thesis a continuous wire is considered so the structure is not important to the calculations.

1.2 Fabrication of Quantum Systems

A few different methods are used to construct nano-scale quantum wires. Firstly, Molecular Beam Epitaxy-growth (MBE) is regularly used in the fabrication of semiconductor devices. MBE takes place in high vacuum and uses slow deposition rate to grow films epitaxially. The high vacuum is necessary for sublimation of the substances that make the film, to take place[5].

A Cleaved-edge Overgrowth is another type of MBE where two separate MBE growths are made with a split in the original place of the substrate the film is being grown upon. This methods is used to create quantum dots

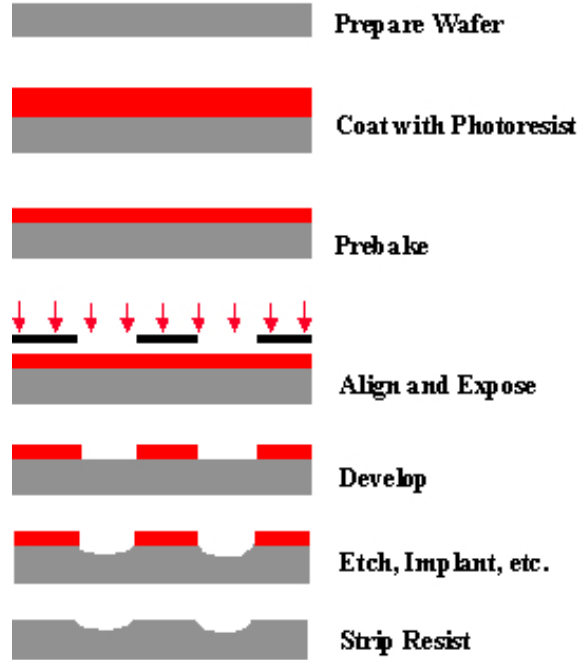


Figure 1.1: Optical lithography explanation [4]

rather than quantum wires.

A Catalytic growth of nanowires is done by letting droplets of some alloys on a substrate and then let the wire grow under the droplet. The shape of the catalyst wire depends on the size of the droplet and therefore, to make a nanowire with this method, some special materials must be used to form the droplet[27].

Nanolithography has many sections where optical lithography has been the predominant technique up until recently. In optical lithography light with short wavelengths is used to remove parts of a film from a substrate to form a pattern, in this case a nanowire. A light sensitive (photoresist) chemical is put on the film on substrate, then a photomask is used to form the preferred pattern. Then the system is exposed to light that removes the photoresist which is lastly exposed to an oxide that doesn't affect the photosensitive chemical, only the film. Finally the rest of the photoresist is removed leaving only the desired shape of film on the substrate. Fig. 1.1 is an explanatory picture of the process. This method is good for nanowires around 100nm width but to make even smaller wires, next generation lithography techniques are required. They are only now being developed but show promising results[25].

Chapter 2

Description of the System

2.1 Quantum Wire

When a wire is of a nanoscale width, small enough for quantum mechanical effects to play a significant role, it's called a quantum wire. Electrons on the two dimensional quantum wire can be approximated as a two dimensional electron gas (2DEG). The theory of the 2DEG has been studied thoroughly in the past[19][21]. When a cross section of the wire is examined, the system can be approximated as a quantum well with hard walls. An additional confinement is often more realistic and can be considered as a perturbation of the hard walls system.

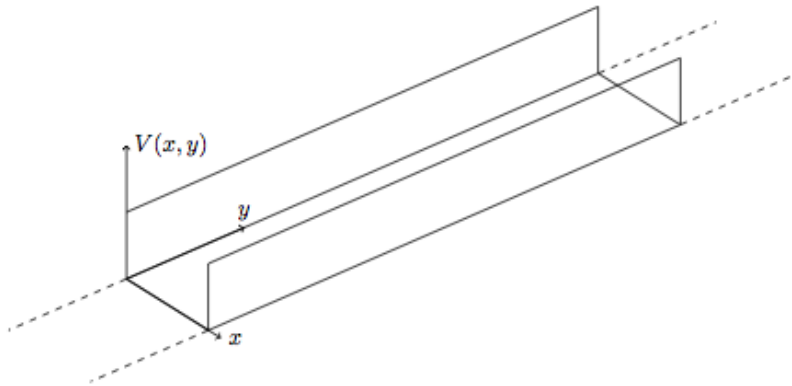


Figure 2.1: A schematic picture of the system.

A schematic of the wire in question can be seen in Fig 2.1. It is considered long enough so the length is infinite compared to the width. The y -axis lies

along the wire, the x -axis across the wire and the z -axis is perpendicular to the wire. The wire is confined within hard walls because realistically confined quantum wires do not have strict walls an additional confinement is also used, either Gaussian, parabolic or linear.

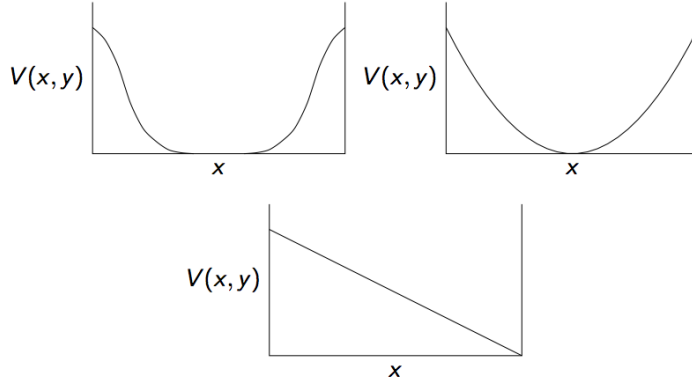


Figure 2.2: A Gaussian confinement to the top left, a parabolic confinement to the top right and linear confinement on the bottom.

2.2 Hamiltonian of a Quantum Wire

The Hamiltonian used to describe this system consist of a few factors. There is a kinetic part that depends on the basic system of infinite quantum well (H_0). A uniform magnetic field is present which introduces a magnetic term to the Hamiltonian (H_B). There is a perturbation in the form of a confinement, either linear, parabolic or Gaussian (V_{conf}). A spin part with the Zeeman term (H_Z) and a spin orbit interaction which is again split into Rashba and Dresselhaus terms ($H_{\text{SOI}} = H_R + H_D$). The final Hamiltonian of the system can be written as

$$H = H_0 + H_B + V_{\text{conf}} + H_Z + H_R + H_D .$$

2.2.1 The Basis States with Hard Walls

The basis wave functions for a system with hard walls are

$$\Psi_{nk}(x, y) = \frac{e^{iky}}{L_y^{1/2}} \varphi_n(x), \quad \varphi_n(x) = \sqrt{\frac{2}{L_x}} \sin \left(\frac{n(x + L_x/2)\pi}{L_x} \right) , \quad (2.1)$$

where the energy is

$$E = \frac{\hbar^2 \pi^2 n^2}{2mL_x^2} + \frac{\hbar^2 k^2}{2m} .$$

The system is translational invariant in the y direction and therefore the wavenumber k is a good quantum number. All the matrix elements of the complete Hamiltonian will be diagonal in k . Periodic boundary conditions are used in the y direction, meaning that we consider k discretized, $k = \frac{2\pi}{L_y} \times \text{integer}$. The basis states will also be denoted as

$$|q\rangle = |nk\sigma\rangle = \varphi_n(x)\varphi_k(y)|\sigma\rangle .$$

2.2.2 Soft Confinement

There are three different confinements used for examining the wire. A Gaussian, linear and parabolic potential. The matrix elements are calculated directly using

$$\begin{aligned} \langle q | V_{\text{conf}} | q' \rangle &= \langle nk\sigma | V_{\text{conf}} | n'k'\sigma' \rangle \\ &= \int_{-L_x/2}^{L_x/2} dx \varphi_n^*(x) V_{\text{conf}}(x) \varphi_n(x) , \end{aligned}$$

where q is the combined quantum number including n, k and σ . The integrals are calculated either numerically (Gaussian) or analytically (parabolic and linear). It is possible to calculate the matrix elements for the Gaussian confinement analytically but it takes up more computational power since the result includes a number of complex error functions[24].

2.2.3 Chemical Potential

The chemical potential has an important role in semiconductor physics and gives one an idea of the transport of charges. It's defined as the change in free energy when electrons are added or removed from a system and usually has the units of energy per particle or meV here.

If N is the number of electrons, \mathcal{F} is the Fermi function and a is a quantum number representing the single particle states of the Hamiltonian for any fixed wavenumber k , then

$$N = \sum_{a,k} \mathcal{F}(E_{ak}) .$$

Now observe that

$$\sum_k \mathcal{F}(E_{ak}) = \int_{-\infty}^{\infty} \frac{dk}{\Delta k} \mathcal{F}(E_{ak}) ,$$

where from the periodic boundary conditions are obtained with $\Delta k = \frac{2\pi}{L_y}$ so

$$N = \sum_a \frac{L_y}{2\pi} \int_{-\infty}^{\infty} dk \mathcal{F}(E_{ak}) = \frac{L_y}{2\pi} \cdot \sum_a I(a)$$

The integrals are found with

$$\begin{aligned} I(a) &= \int_{-\infty}^{\infty} dk \mathcal{F}(E_{ak}) \\ &= 2 \int_0^{\infty} dk \mathcal{F}(E_{ak}) \\ &= 2 \sum_{j=0}^{N_k-1} (k_{j+1} - k_j) \frac{\mathcal{F}(E_{ak_j}) + \mathcal{F}(E_{ak_{j+1}})}{2} \\ &= 2 \frac{k_{y\max}}{N_k} \left[\frac{1}{2} \left(\mathcal{F}(E_{ak_0}) + \mathcal{F}(E_{ak_{N_k}}) \right) + \sum_{j=1}^{N_k-1} \mathcal{F}(E_{ak_j}) \right] , \end{aligned}$$

where $k_{y\max}$ is a sufficiently large cutoff and N_k is the total number of k value. This is a separate discretisation of the k space and not the one implied by the boundary conditions, which were used in the integration. Now since

$$\mathcal{F}(E) = \frac{1}{e^{(E-\mu)/k_B T} + 1} ,$$

where μ is the chemical potential and the average electron density is

$$\frac{N}{L_x L_y} = \frac{1}{2\pi L_x} \sum_a I(a) .$$

These equations are used to calculate the chemical potential numerically[16]. The average electron density is a fixed parameter in our evaluations with the size $2 \cdot 10^{11} \text{cm}^{-1}$.

2.2.4 Magnetic field

In a uniform magnetic field, using the Landau gauge the Hamiltonian is

$$H = H_0 + H_B = \frac{P_x^2}{2m} + \frac{(P_y + eA_y)^2}{2m},$$

with

$$H_B = \frac{e}{m} A_y P_y + \frac{e^2}{2m} A_y^2.$$

The magnetic term of the Hamiltonian can be split into two parts, proportional to x and x^2 . First there is

$$H_{B_1} = \frac{eB}{m} x P_y = i\hbar\omega_c x \partial_y,$$

and then

$$H_{B_2} = \frac{\hbar\omega_c}{2l^2} x^2,$$

where $l = \left(\frac{\hbar}{eB}\right)^{1/2}$ as before. The matrix elements of the magnetic part are

$$\langle q | H_{B_1} | q' \rangle = \langle nk\sigma | i\hbar\omega_c x \partial_y | n'k'\sigma' \rangle = -\hbar\omega_c k \delta_{kk'} \delta_{\sigma\sigma'} \langle n | x | n' \rangle$$

and

$$\langle q | H_{B_2} | q' \rangle = \left\langle nk\sigma \left| \frac{\hbar\omega_c}{2l_B^2} x^2 \right| n'k'\sigma' \right\rangle = \frac{\hbar\omega_c}{2l_B^2} \delta_{kk'} \delta_{\sigma\sigma'} \langle n | x^2 | n' \rangle.$$

To calculate the brackets the following is used

$$\langle n | x^m | n' \rangle = L_x^m \text{I2s}(m; -\pi/2; n, n').$$

Calculations for the I2s function can be found in an appendix A.1.

2.2.5 Zeeman term

The Zeeman term of the Hamiltonian is according to ref. [9]

$$H_Z = -\frac{1}{2} \gamma \hbar \omega_c \hat{\sigma}_z,$$

where

$$\gamma = \frac{1}{2} g^* \frac{m^*}{m},$$

where g^* is the g-factor of the material being used and m^* is the effective mass. The matrix elements are

$$\langle nk\sigma | H_Z | n'k'\sigma' \rangle = \delta_{nn'} \delta_{kk'} \left(-\frac{1}{2} \gamma \hbar \omega_c \sigma \right) \delta_{\sigma\sigma'}, \quad \sigma = \pm 1.$$

Chapter 3

Spin-Orbit Interaction

The spin-orbit interaction (SOI) has two terms. The Rashba term $H_R = \frac{\alpha}{\hbar} (\sigma_x p_y - \sigma_y p_x)$ [10, 12] and the Dresselhaus term $H_D = \frac{\beta}{\hbar} (\sigma_x p_x - \sigma_y p_y)$ [13]. Here α and β are material constants that give the strength of the SOI. The SOI can also be changed by an external electric field. The σ_i are Pauli matrices and the $p_j = -i\hbar\partial_j$ are momenta. Three different materials are considered, GaAs, InAs and InSb. Besides having different SOI parameters they also differ in effective mass m^* , effective g-factor g^* and dielectric constant κ .

The matrix elements of the Rashba term are

$$\begin{aligned} \langle \varphi_q | H_R | \varphi_{q'} \rangle &= \langle nk\sigma | H_R | n'k'\sigma' \rangle \\ &= \frac{\alpha}{\hbar} \int \int dx dy \varphi_n^*(x) \varphi_k^*(y) \langle \sigma | \sigma_x p_y - \sigma_y p_x | \sigma' \rangle \varphi_{n'}(x) \varphi_{k'}(y) \\ &= \frac{\alpha}{\hbar} [(\sigma_x)_{\sigma\sigma'} \langle nk | p_y | n'k' \rangle - (\sigma_y)_{\sigma\sigma'} \langle nk | p_x | n'k' \rangle] , \end{aligned}$$

where q includes also the spin quantum number σ as well as n and k . Using the basis functions in the x and y directions, already mentioned in Eq. 2.1

	GaAs	InAs	InSb
m^*	0.067	0.023	0.014
κ	12.4	14.6	17.9
g^*	-0.44	-14.9	-51.6
α	1.0	20.0	50.0
β	3.0	3.0	30.0

Table 3.1: Material constants for GaAs, InAs and InSb. The dimensions of α and β are meVnm, the other parameters are dimensionless.

$$\begin{aligned}
\langle nk | p_x | n' k' \rangle &= -i\hbar \int_0^{L_x} dx \int dy \varphi_n^*(x) \varphi_k^*(y) (\partial_x \varphi_{n'}(x)) \varphi_{k'}(y) \\
&= -i\hbar \delta_{kk'} \int_0^{L_x} dx \left(\sqrt{\frac{2}{L_x}} \sin\left(\frac{n\pi x}{L_x}\right) \right) \left(\sqrt{\frac{2}{L_x}} \frac{n'\pi}{L_x} \cos\left(\frac{n'\pi x}{L_x}\right) \right) .
\end{aligned}$$

Now, the integral is

$$\begin{aligned}
&\int_0^{L_x} dx \left(\sqrt{\frac{2}{L_x}} \sin\left(\frac{n\pi x}{L_x}\right) \right) \left(\sqrt{\frac{2}{L_x}} \frac{n'\pi}{L_x} \cos\left(\frac{n'\pi x}{L_x}\right) \right) \\
&= \frac{n'}{L_x} \left[1 - (-1)^{n+n'} \right] \left(\frac{1}{n+n'} + \frac{1}{n-n'} \right) ,
\end{aligned}$$

and thus

$$\langle nk | p_x | n' k' \rangle = -i\hbar \delta_{kk'} \left[1 - (-1)^{n+n'} \right] \frac{2nn'}{n^2 - n'^2} \cdot \frac{1}{L_x} ,$$

which equals zero for $n = n'$.

In a similar way the matrix elements of the momentum in y direction are obtained with

$$\langle nk | p_y | n' k' \rangle = \hbar k \delta_{nn'} \delta_{kk'} .$$

Obviously the matrix elements of momentum operators are diagonal in spin, and so the label σ was omitted.

The matrix elements of the Rashba term are

$$\langle q | H_R | q' \rangle = \alpha \left[(\sigma_x)_{\sigma\sigma'} k \delta_{nn'} - (\sigma_y)_{\sigma\sigma'} \frac{i}{L_x} g_{nn'} \right] \delta_{kk'} ,$$

where

$$g_{nn'} = \left[1 - (-1)^{n+n'} \right] \frac{2nn'}{n^2 - n'^2} = \begin{cases} 0 & \text{for } n + n' \text{ even} \\ \frac{4nn'}{n^2 - n'^2} & \text{for } n + n' \text{ odd} \end{cases} .$$

The matrix elements due to the Dresselhaus term can be found in a similar fashion. That is

$$\langle q | H_D | q' \rangle = \frac{\beta_D}{\hbar} [(\sigma_x)_{\sigma\sigma'} \langle n | p_x | n' \rangle - (\sigma_y)_{\sigma\sigma'} (\hbar k \delta_{nn'} + eB \langle n | x | n' \rangle)] \delta_{kk'} ,$$

and calculations for $\langle n | p_x | n' \rangle$ and $\langle n | x^m | n' \rangle$ can be found above and in an appendix A.1.

Chapter 4

Charge and Spin Densities

4.1 Operators and Expected Values

The charge density according to ref. [16] is

$$\rho(x, y) = \rho(x) = \sum_{ak} \mathcal{F}_{ak} |\psi_{ak}|^2 .$$

Again using the periodic boundary conditions along y one can write the summation over k as an integraion

$$\rho(x) = \frac{L_y}{2\pi} \sum_a \int dk \mathcal{F}_{ak} |\psi_{ak}|^2 = \sum_{qq'} \varphi_n^*(x) \varphi_{n'}(x) \delta_{\sigma\sigma'} \text{Gmat}(q, q') .$$

Here the notation $\text{Gmat}(q, q')$ is an integral explained in appendix A.2 with the rest of these calculations. Note that here q and q' contain the orbital and spin quantum numbers n and σ respectively so that the double summation includes both n and σ .

The spin density is

$$\mathbf{s}(x) = \sum_{ak} \mathcal{F}_{ak} \langle ak | \mathbf{S} | ak \rangle = \frac{\hbar}{2} \sum_{ak} \mathcal{F}_{ak} \langle \psi_{ak} | \boldsymbol{\sigma} | \psi_{ak} \rangle .$$

With $i = x, y, z$ the spin densities corresponding to each polarization direction can be written as

$$s_i(x) = \frac{\hbar}{2} \sum_{ak} \mathcal{F}_{ak} \psi_{ak}^\dagger \sigma_i \psi_{ak} .$$

By expanding the wave functions the spin densities become

$$s_i(x) = \sum_{qq'} \varphi_n^*(x) \varphi_{n'}(x) \frac{\hbar}{2} (\sigma_i)_{\sigma\sigma'} \text{Gmat}(q, q') .$$

Formally the previous result for the electron density can be obtained by replacing the spin with 1.

$$\frac{\hbar}{2} (\sigma_i)_{\sigma\sigma'} \rightarrow \delta_{\sigma\sigma'} \Rightarrow s_i(x) = \rho(x) .$$

4.2 SOI Effects on the Spin Polarization

By looking at different SOI a difference in spin polarization is studied. In Fig. 4.1 an InAs quantum wire is studied with only Rashba SOI. On the left there is the energy spectrum of the wire with the chemical potential shown. On the right side from the top down there is charge density and x, y, z spin densities respectively. Since there is only a Rashba SOI ($\beta_D = 0$), the y spin density is zero for all x . In Fig. 4.2 on the other hand there is only a Dresselhaus SOI ($\alpha_R = 0$) so the y spin becomes zero. In both cases the spin z density is symmetric while the spin x and then spin y densities are anti-symmetric across the wire. In other words $s_x(x) = -s_x(-x)$ and $s_y(x) = -s_y(-x)$, but $s_z(x) = s_z(-x)$. This is true only with the magnetic field in the z direction, i.e. perpendicular to the wire. Obviously, in the absence of both SOI's the in-plane spin components would vanish, i. e. $s_x = s_y = 0$. The energy spectrum is symmetric, i. e. an even function of $E_{a,k} = E_{a,-k}$, and the particle density is also an even function of x , $\rho(x) = \rho(-x)$ due to the left-right symmetry of the lateral confinement of the quantum wire.

In Figs. 4.3 and 4.4 the magnetic field is not perpendicular to the wire, but along the wire (i. e. along the y direction), and across the wire (i. e. along the x direction) respectively. In both cases the energy spectrum becomes narrower than with the magnetic field perpendicular to the wire. It should also be noted that the energy spectrum is no longer symmetric in the k space: the minima of each energy band shift in opposite directions, down-left and up-right, respectively, due to the Zeeman effect in the y or x directions. However, the charge density remains symmetric. The system still has lateral symmetry (left-right) which is not changed by the SOI. But now the symmetry of the spin densities is different from the previous case with B in the z direction. In both cases, with the in plane magnetic field, either along or across the wire, the spin z density is anti-symmetric whereas the spin x, y densities are symmetric.

In Fig. 4.5 there are both Rashba and Dresselhaus SOI in a strong parabolic confinement. The noticeable difference between Figs. 4.5 and 4.6 which are obtained with parabolic confinement and Gaussian confinement, respectively but otherwise same parameters, is the spectra become more scattered with the parabolic confinement and the densities become more centered. Notice also that shoulders of the electron density seen in the Gaussian confinement vanishes in the parabolic confinement.

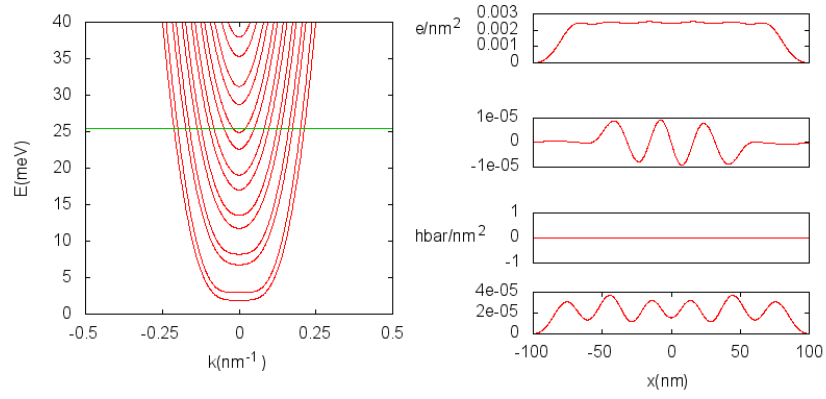


Figure 4.1: Energy spectrum, charge and spin densities for InAs wire and Rashba effects. The green horizontal line represents the chemical potential. $\rho(x) = \rho(-x)$ where $\rho(x) = en(x) - e\langle n \rangle$.

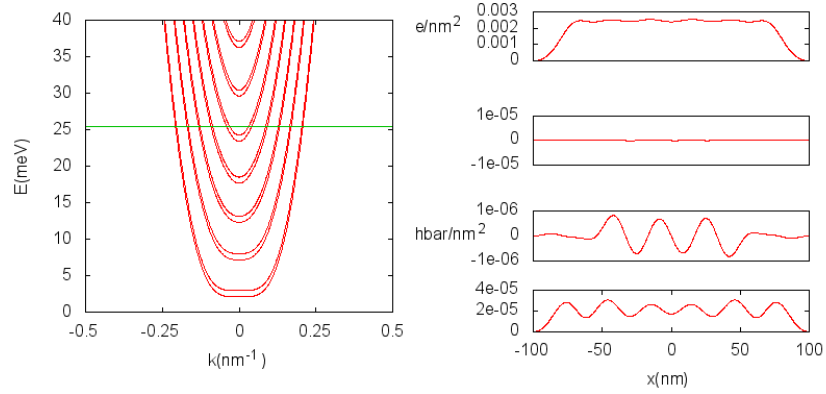


Figure 4.2: Energy spectrum, charge and spin densities for InAs wire and Dresselhaus effects.

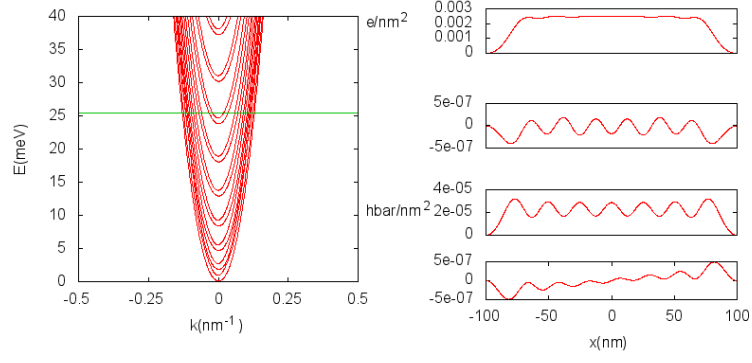


Figure 4.3: Spectrum and densities of an InAs wire with both SOI and magnetic field along the wire.

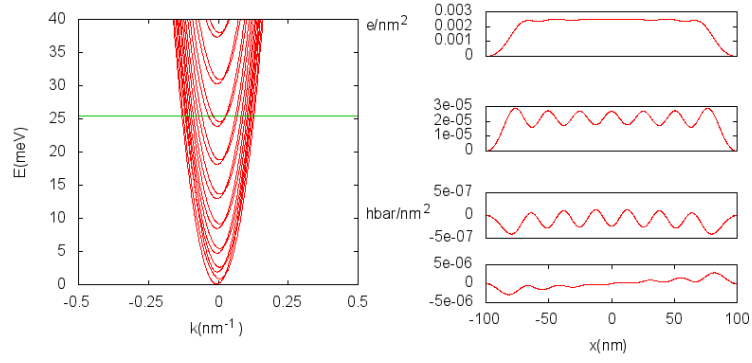


Figure 4.4: Spectrum and densities of an InAs wire with both SOI and magnetic field across the wire.

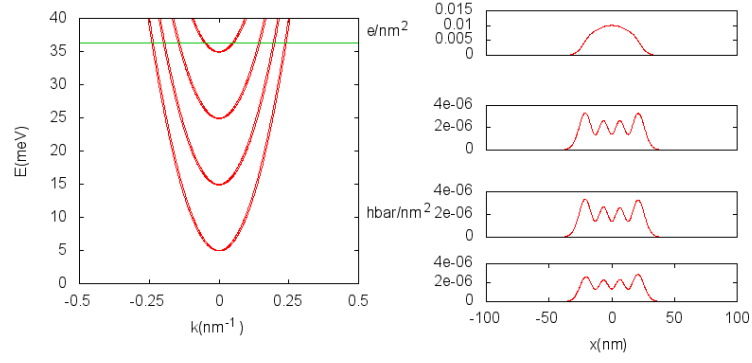


Figure 4.5: Spectrum and densities of a GaAs wire in a parabolic confinement.

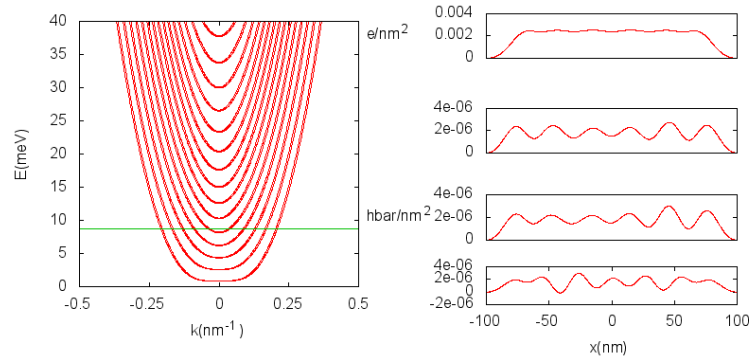


Figure 4.6: Spectrum and densities of a GaAs wire in a Gaussian confinement.

Chapter 5

Charge and Spin Currents

5.1 Current Density Operators

The current density operator for charge current density is

$$\mathbf{J}(\mathbf{r}) = \frac{1}{2} [\delta(\mathbf{r} - \mathbf{r}_0) e \mathbf{v} + \text{h.c.}] ,$$

and for the spin current density it is

$$\mathbf{J}_\mu(\mathbf{r}) = \frac{1}{2} \left[\delta(\mathbf{r} - \mathbf{r}_0) \left(\frac{\hbar}{2} \sigma_\mu \right) \mathbf{v} + \text{h.c.} \right] ,$$

where \mathbf{r} is the observable position, \mathbf{r}_0 is the particle position and $\mathbf{v} = \mathbf{v}(\mathbf{r}_0)$ is the velocity operator. The notation h.c. means the Hermitian conjugate which guarantees real values of the expected values of the current. Here μ equals 0, x , y or z . If $\mu = 0$ the equation for spin current density becomes the equation for charge current density where $\sigma_0 = \frac{2}{\hbar} e$.

Now, the velocity operator is the time derivative of the position

$$\mathbf{v}(\mathbf{r}) = \dot{\mathbf{r}} = \frac{1}{i\hbar} [\mathbf{r}, \hat{H}] .$$

5.2 Expectation Value of Current Densities

For a current density in the direction y , along the wire, the expectation value for the operator according to ref. [24] is

$$\langle \mathbf{J}_\mu \rangle = \sum_{ak} \mathcal{F}_{ak} \langle ak | \mathbf{J}_\mu | ak \rangle .$$

The bracket can be written as

$$\begin{aligned}
\langle ak | \mathbf{J}_\mu(\mathbf{r}) | ak \rangle &= \frac{1}{2} \frac{\hbar}{2} \int d\mathbf{r}_0 \psi_{ak}^\dagger(\mathbf{r}_0) \left[\underbrace{\delta(\mathbf{r} - \mathbf{r}_0) \sigma_\mu \mathbf{v}(\mathbf{r}_0)}_{\mathbf{A}} + \underbrace{\mathbf{v}(\mathbf{r}_0) \sigma_\mu \delta(\mathbf{r} - \mathbf{r}_0)}_{\mathbf{A}^\dagger} \right] \psi_{ak}(\mathbf{r}_0) \\
&= \frac{1}{2} \frac{\hbar}{2} \psi_{ak}^\dagger(\mathbf{r}) (\sigma_\mu \mathbf{v}(\mathbf{r}) + \mathbf{v}(\mathbf{r}) \sigma_\mu) \psi_{ak}(\mathbf{r}) \\
&= \frac{1}{2} \frac{\hbar}{2} \langle ak | \sigma_\mu \mathbf{v}(\mathbf{r}) + \mathbf{v}(\mathbf{r}) \sigma_\mu | ak \rangle .
\end{aligned} \tag{5.1}$$

Using the \mathbf{A} notation from Eq. 5.1

$$\langle ak | \mathbf{A} + \mathbf{A}^\dagger | ak \rangle = \langle ak | \mathbf{A} | ak \rangle + \langle ak | \mathbf{A} | ak \rangle^* = 2\Re \langle ak | \mathbf{A} | ak \rangle ,$$

that is

$$\langle \mathbf{J}_\mu \rangle = \frac{\hbar}{2} \sum_{ak} \mathcal{F}_{ak} \Re (\langle ak | \sigma_\mu \mathbf{v} | ak \rangle) .$$

The projections for the spin are calculated by expanding the wave functions in the basis from Eq. 2.1

$$\begin{aligned}
|ak\rangle &= \psi_{ak}(\mathbf{r}) = \sum_{n\sigma} c_a(nk\sigma) \varphi_{nk}(\mathbf{r}) |\sigma\rangle \\
\langle \sigma | ak \rangle &= \psi_{ak}(\mathbf{r}, \sigma) = \sum_n c_a(nk\sigma) \varphi_{nk}(\mathbf{r}) \\
\langle ak | \sigma \rangle &= \psi_{ak}^\dagger(\mathbf{r}, \sigma) = \sum_n c_a^\dagger(nk\sigma) \varphi_{nk}^\dagger(\mathbf{r}) ,
\end{aligned}$$

which gives

$$\begin{aligned}
\langle \mathbf{J}_\mu \rangle &= \frac{\hbar}{2} \sum_{ak} \mathcal{F}_{ak} \Re \sum_{\sigma_1 \sigma_2} \langle ak | \sigma_1 \rangle \langle \sigma_1 | \sigma_\mu \mathbf{v} | \sigma_2 \rangle \langle \sigma_2 | ak \rangle \\
&= \frac{\hbar}{2} \sum_{ak} \mathcal{F}_{ak} \Re \sum_{\sigma_1 \sigma_2} \psi_{ak}^*(\mathbf{r}, \sigma_1) (\sigma_\mu \mathbf{v})_{\sigma_1 \sigma_2} \psi_{ak}(\mathbf{r}, \sigma_2) .
\end{aligned}$$

Now the current density along the wire (in the y direction) is

$$\langle J_\mu(x) \rangle = \frac{\hbar}{2} \sum_{ak} \mathcal{F}_{ak} \Re \sum_{\sigma_1 \sigma_2} \psi_{ak}^*(\mathbf{r}, \sigma_1) (\sigma_\mu v_y)_{\sigma_1 \sigma_2} \psi_{ak}(\mathbf{r}, \sigma_2) ,$$

where

$$\psi_{ak}(\mathbf{r}, \sigma) = \psi_{ak}(x, \sigma) \frac{1}{\sqrt{L_y}} e^{iky} ,$$

and

$$v_y = \dot{y} = \frac{1}{i\hbar} [y, H] \ .$$

Below one can see figures with spectra and current densities for GaAs and InAs with either magnetic field perpendicular to the wire or along the wire. In the case where the magnetic field is perpendicular to the wire ($B_z = 1\text{T}$) the charge current density and the spin z current density are anti-symmetric while spin x, y current densities are symmetric. When the magnetic field is along the wire the only density that's anti-symmetric is the spin z current density. It's also worth to note that the densities have higher amplitudes when the magnetic field is perpendicular to the wire. This holds for both GaAs and InAs.

Next, in Fig. 5.3 we show one example of current densities for InAs with the magnetic field in the y direction, with the same parameters as in Fig. 4.3. The charge-current density is left-right symmetric, just like the charge density. However the total charge-current, i. e. the integral of the data shown, is zero, although not obvious from the figure, but consistent with the physical situation: the in-plane magnetic field does not influence the orbital motion and cannot induce a net current. The spin currents have also the same symmetry as the spin densities, and the net currents with x and y polarization are not zero, whereas the one with z polarization is zero. The same results are obtained for an in-plane magnetic field oriented along the x direction, as shown in Fig. 5.4. Obviously, the spin currents with x and y polarization are possible (not zero) only in the presence of SOI. In Fig. 5.5 both the spin polarizations and densities are shown to demonstrate the symmetry and antisymmetry.

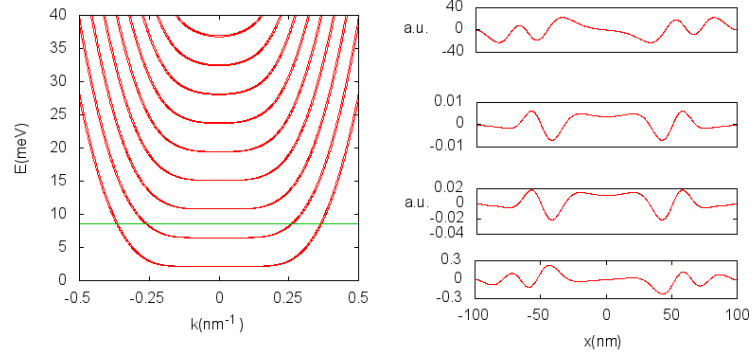


Figure 5.1: Spectrum and current densities with magnetic field perpendicular to the GaAs wire. The currents are given in arbitrary units (a.u.). The panels on the right hand side from top to bottom charge current density and spin current x, y, z densities.

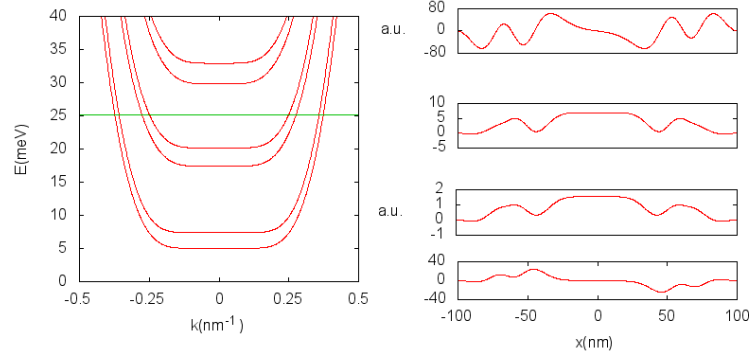


Figure 5.2: Spectrum and current densities with magnetic field perpendicular to the InAs wire. The currents are given in arbitrary units (a.u.). The panels on the right hand side from top to bottom charge current density and spin current x, y, z densities.

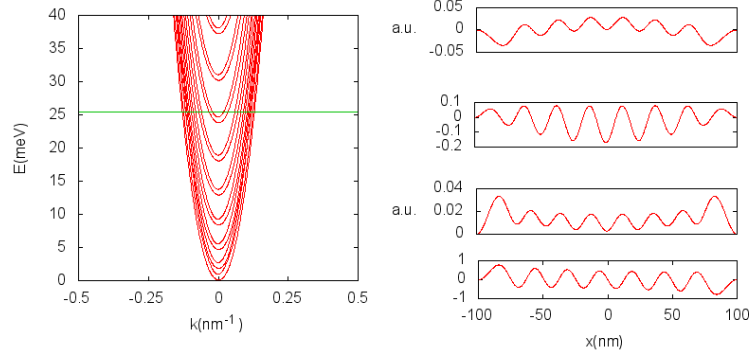


Figure 5.3: Spectrum and current densities with magnetic field along the InAs wire. The currents are given in arbitrary units (a.u.). The panels on the right hand side from top to bottom charge current density and spin current x, y, z densities.

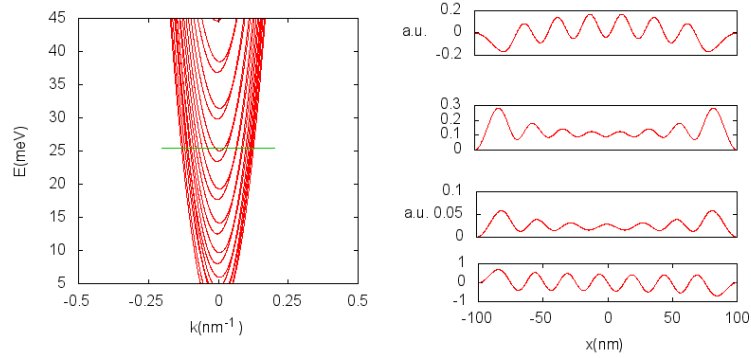


Figure 5.4: Spectrum and current densities with magnetic field across the InAs wire. The currents are given in arbitrary units (a.u.). The panels on the right hand side from top to bottom charge current density and spin current x, y, z densities.

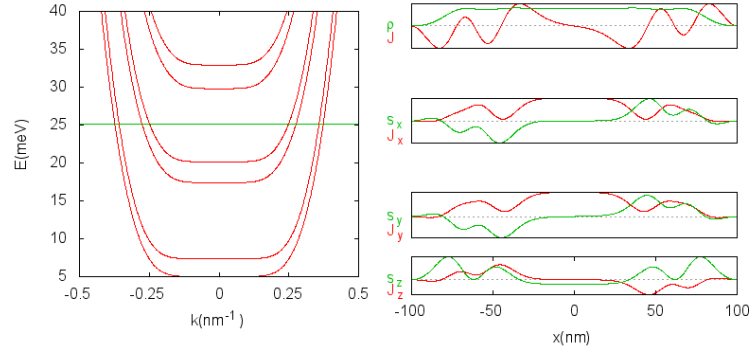


Figure 5.5: Spectrum with both densities (green) and current densities (red) with magnetic field perpendicular to the InAs wire. The currents are given in arbitrary units (a.u.). The panels on the right hand side from top to bottom charge current density and spin current x, y, z densities.

Chapter 6

Coulomb Interaction

6.1 Hartree-Fock

For these calculations the Hartree-Fock approximation was used to describe the Coulomb interaction in the system. The Hartree-Fock method gives an approximate solution to the Coulomb effects in a many electron system by assuming that the many body wave function of the system can be found approximately with a single Slater determinant[18, 16]. The Hartree-Fock method was chosen over other methods such as density functional theory (DFT), since SOI is not implemented rigorously in DFT formalism that we are aware of even though there are attempts in progress[7, 20]. In this thesis the Hartree term will refer to the direct component of the Coulomb interaction and Fock will refer to the exchange term.

The effective Hamiltonian for Hartree-Fock method can be written as

$$H = H_0 + \Sigma_{HF} ,$$

according to ref. [16], where H_0 is the Hamiltonian without Coulomb interaction and Σ_{HF} is the Hartree-Fock self energy. The self energy has a non-local expression so the Schrödinger equation can be written as

$$H\psi_a = E_a\psi_a \Rightarrow (H_0 + \Sigma_{HF})\psi_a = E_a\psi_a ,$$

where the wave number k is treated as a hidden parameter. The reason is that the Coulomb interaction does not change the translational invariance of the quantum wire in the y direction and k remains a good quantum number. The action of the self energy on any wave function is

$$\Sigma_{HF}(\mathbf{r})\varphi(\mathbf{r}) = \int d\mathbf{r}' \Sigma_{HF}(\mathbf{r}, \mathbf{r}')\varphi(\mathbf{r}') .$$

The self energy can be split into direct and exchange term where

$$\Sigma_{HF}(\mathbf{r}, \mathbf{r}') = \Sigma_H(\mathbf{r}, \mathbf{r}') + \Sigma_F(\mathbf{r}, \mathbf{r}') .$$

Now it is possible to write the self energy for the direct and exchange term respectively, as

$$\Sigma_H(\mathbf{r}, \mathbf{r}') = \delta(\mathbf{r} - \mathbf{r}') \int d\mathbf{r}_1 u(\mathbf{r}_1 - \mathbf{r}) \rho(\mathbf{r}_1) = \delta(\mathbf{r} - \mathbf{r}') V_H(\mathbf{r}) ,$$

and

$$\Sigma_F(\mathbf{r}, \mathbf{r}') = -u(\mathbf{r} - \mathbf{r}') \sum_a \mathcal{F}_a \psi_a(\mathbf{r}) \psi_a^\dagger(\mathbf{r}') ,$$

where u the Coulomb potential and ρ is the charge density and is defined as $\rho(x) = en(x) - e\langle n \rangle$ where the second term corresponds to a positive background of charge, the ionized donors which injected electrons into the 2D layer. This guarantees the charge neutrality of the system.

With the basis vector $|q\rangle = |n\sigma\rangle = \varphi_{n\sigma}(\mathbf{r}) = \varphi_n(\mathbf{r}) |\sigma\rangle$, where $\varphi_n(\mathbf{r})$ is a scalar wave function, the matrix elements of the direct term are

$$\begin{aligned} \langle n_1 \sigma_1 | \Sigma_H | n_2 \sigma_2 \rangle &= \int d\mathbf{r} \varphi_{n_1 \sigma_1}^\dagger(\mathbf{r}) V_H(\mathbf{r}) \varphi_{n_2 \sigma_2}(\mathbf{r}) \\ &= \int d\mathbf{r} \varphi_{n_1}^*(\mathbf{r}) \langle \sigma_1 | V_H(\mathbf{r}) | \sigma_2 \rangle \varphi_{n_2}(\mathbf{r}) \\ &= \int d\mathbf{r} \varphi_{n_1}^*(\mathbf{r}) V_H(\mathbf{r}) \varphi_{n_2}(\mathbf{r}) \delta_{\sigma_1 \sigma_2} . \end{aligned}$$

This can also be written as

$$\langle n_1 \sigma_1 | \Sigma_H | n_2 \sigma_2 \rangle = \int d\mathbf{r} d\mathbf{r}' \varphi_{n_1 n_2}^\dagger(\mathbf{r}) u(\mathbf{r} - \mathbf{r}') \rho(\mathbf{r}') \varphi_{n_1 n_2}(\mathbf{r}) .$$

Now

$$\rho(\mathbf{r}) = \sum_a \mathcal{F}_a \psi_a^\dagger(\mathbf{r}) \psi_a(\mathbf{r}) - \langle \rho \rangle ,$$

so

$$\begin{aligned} \langle n_1 \sigma_1 | \Sigma_H | n_2 \sigma_2 \rangle &= \\ &= \sum_a \mathcal{F}_a \int d\mathbf{r} d\mathbf{r}' \varphi_{n_1 \sigma_1}^\dagger(\mathbf{r}) \psi_a^\dagger(\mathbf{r}') u(\mathbf{r} - \mathbf{r}') \psi_a(\mathbf{r}') \varphi_{n_2 \sigma_2}(\mathbf{r}') \\ &= \sum_a \mathcal{F}_a \sum_{\substack{m_1 \zeta_1 \\ m_2 \zeta_2}} c_{a, m_1 \zeta_1}^* c_{a, m_2 \zeta_2} \int d\mathbf{r} d\mathbf{r}' \varphi_{n_1 \sigma_1}^\dagger(\mathbf{r}) \varphi_{m_1 \zeta_1}(\mathbf{r}') u(\mathbf{r} - \mathbf{r}') \varphi_{m_2 \zeta_2}(\mathbf{r}') \varphi_{n_2 \sigma_2}(\mathbf{r}) \\ &= \delta_{\sigma_1 \sigma_2} \sum_a \mathcal{F}_a \sum_{\substack{m_1 m_2 \\ \zeta_1 \zeta_2}} (c_{a, m_1 \zeta_1}^* c_{a, m_2 \zeta_2} \delta_{\zeta_1 \zeta_2}) \int d\mathbf{r} d\mathbf{r}' \varphi_{n_1}^*(\mathbf{r}) \varphi_{m_1}^*(\mathbf{r}') u(\mathbf{r} - \mathbf{r}') \varphi_{m_2}(\mathbf{r}') \varphi_{n_2}(\mathbf{r}) . \end{aligned}$$

These are the matrix elements of the direct self energy where m_1 and m_2 include the wave number.

The matrix elements of the self energy for the exchange term are

$$\begin{aligned}
\langle n_1 \sigma_1 | \Sigma_F | n_2 \sigma_2 \rangle &= \int d\mathbf{r} d\mathbf{r}' \varphi_{n_1 \sigma_1}^\dagger(\mathbf{r}) \Sigma_F(\mathbf{r}, \mathbf{r}') \varphi_{n_2 \sigma_2}(\mathbf{r}') \\
&= \int d\mathbf{r} d\mathbf{r}' \varphi_{n_1}^*(\mathbf{r}) \langle \sigma_1 | \Sigma_F(\mathbf{r}, \mathbf{r}') | \sigma_2 \rangle \varphi_{n_2}(\mathbf{r}') \\
&= - \sum_{ak} \mathcal{F}_{ak} \int d\mathbf{r} d\mathbf{r}' \varphi_{n_1 \sigma_1}^\dagger(\mathbf{r}) \psi_{ak}(\mathbf{r}) u(\mathbf{r} - \mathbf{r}') \psi_{ak}^\dagger(\mathbf{r}') \varphi_{n_2 \sigma_2}(\mathbf{r}') \\
&= - \sum_{ak} \mathcal{F}_{ak} \int d\mathbf{r} d\mathbf{r}' \varphi_{n_1 \sigma_1}^\dagger(\mathbf{r}) \psi_{ak}^\dagger(\mathbf{r}') u(\mathbf{r} - \mathbf{r}') \psi_{ak}(\mathbf{r}) \varphi_{n_2 \sigma_2}(\mathbf{r}') ,
\end{aligned}$$

which gives

$$\begin{aligned}
&\langle n_1 \sigma_1 | \Sigma_F | n_2 \sigma_2 \rangle = \\
&= - \sum_a \mathcal{F}_a \sum_{\substack{m_1 \zeta_1 \\ m_2 \zeta_2}} c_{a, m_1 \zeta_1} c_{a, m_2 \zeta_2}^* \int d\mathbf{r} d\mathbf{r}' \varphi_{n_1 \sigma_1}^\dagger(\mathbf{r}) \varphi_{m_1 \zeta_1}(\mathbf{r}) u(\mathbf{r} - \mathbf{r}') \varphi_{m_2 \zeta_2}(\mathbf{r}') \varphi_{n_2 \sigma_2}(\mathbf{r}') \\
&= - \sum_a \mathcal{F}_a \sum_{m_1 m_2} (c_{a, m_1 \sigma_1} c_{a, m_2 \sigma_2}^*) \int d\mathbf{r} d\mathbf{r}' \varphi_{n_1}^*(\mathbf{r}) \varphi_{m_1}(\mathbf{r}) u(\mathbf{r} - \mathbf{r}') \varphi_{m_2}^*(\mathbf{r}') \varphi_{n_2}(\mathbf{r}') .
\end{aligned}$$

Here $u(\mathbf{r} - \mathbf{r}')$ is the Coulomb interaction potential

$$u(\mathbf{r} - \mathbf{r}') = \frac{e^2}{\kappa |\mathbf{r} - \mathbf{r}'|} ,$$

after carrying the integrations in the y direction in the matrix elements of the Coulomb self energy one obtains the simplified form

$$\frac{e^2}{\kappa L_x} \ln \left(\frac{|x - x'|}{L_x} \right) .$$

This potential corresponds to the interaction of lines of charge infinitely long in the y direction.

6.2 Effects of Coulomb Interactions on Energy Spectra, Densities and Currents

With the Coulomb interaction the single particle energies increase due to the repulsion between electrons as can be easily noticed in the figures below.

This effect corresponds to the direct Hartree term. In addition the Coulomb repulsion pushes the electrons towards the edges of the wire, in the positive and negative x direction, such that the density profile has lateral maxima, but flattens out in the center of the wire, as shown in Fig. 6.2 top left. The lateral "ears" of the charge density correspond to lateral minima of the self-consistent electrostatic potential (not shown)[1, 2, 3]. The relative height of the lateral maxima may also depend on the steepness of the lateral confinement. They are more prominent with our choice, i. e. the Gaussian lateral walls, but less pronounced if a parabolic confinement would be considered. Because of the lateral peaks of the charge density the energy spectrum forms a sort of pockets on either side and a hill in the middle of the spectrum in k space. This is noticeable with only the direct term of Coulomb (Fig. 6.1) but even more pronounced with both the direct and the exchange term. By including the exchange term (HFA) the slope of the spectra increases near the intersections of the energy bands with the chemical potential shown by the arrows. The reason is the negative sign of the exchange self energy and the short range nature of exchange[22]. A negative amount of energy is thus added to all states with a given wave number k , but self-consistent with the number of occupied states with that particular k .

Another consequence of the increased energy dispersion due to the exchange interaction can be the increase of the otherwise tiny spin gap of GaAs[23]. This situation is known as exchange-enhancement of the spin splitting and was studied initially in the 70's by Ando and Uemura for the homogeneous two-dimensional electron gas in perpendicular magnetic field[28]. The analog effect in the presence of lateral potentials was also studied in several papers using Hartree-Fock theory[23] or density-functional methods[7]. To the best of our knowledge the spin-orbit interaction has never been taken into consideration in this problem. In Fig. 6.2(b-d) the spin densities projected on the x, y, z directions across the quantum wire are shown, in the three approximations: noninteracting (NI) case, Hartree (HA), and the Hartree-Fock approximations (HFA). The spin polarization is enhanced by the exchange interaction in all directions. In other words, not only the g factor is renormalized by the Coulomb effect, but also the strengths of the SOI's, i.e. the Rashba and the Dresselhaus coupling constants. Clearly the magnitude of the spin polarization depends on the relative position of the chemical potential within the energy spectrum, which changes with the magnetic field (to be shown later).

Fig. 6.3 shows amplification of the spin currents since they are proportional to the steepness of the slope. In Fig. 6.4 the energy spectra are compared without and with Coulomb interaction for a quantum wire with ma-

terial parameters of InAs, and a perpendicular magnetic field of $B=3.5$ T. As one can see the exchange interaction (HFA) has a relatively smaller effect than for GaAs (Fig. 6.4). As was mentioned the exchange interaction essentially functions like a short-range potential with a range of the order of the localization length of the electrons, i. e. the spatial extension of the single particle wave functions. For example, assuming a quantum wire with a parabolic confinement of frequency ω , the wave functions behave in the x direction like oscillator wave functions, with spatial extension proportional to $\lambda = \sqrt{\hbar/(m_{eff} \omega)}$. Therefore on the one hand the exchange effects are expected to be roughly proportional to $\lambda^{-1} \sim \sqrt{m_{eff}}$, in principle irrespective of the soft confinement potential. On the other hand the confinement itself creates energy gaps proportional to $1/m_{eff}$ without the Coulomb interaction. So roughly speaking the exchange effects will relatively vanish when the effective mass decreases, as it happens for InAs with $m_{eff} = 0.023$ compared to the GaAs with $m_{eff} = 0.067$. Therefore the steepness of the energy dispersion is much less affected by the exchange in InAs. And obviously, since the bare g factor is already much bigger than in GaAs the spin gap is only barely enhanced in InAs, at least for this quantum wire and magnetic field strengths. Therefore Coulomb effects on spin polarization for InAs, and for InSb as well ($m_{eff} = 0.014$) if any, can be attributed to the direct, Hartree interaction.

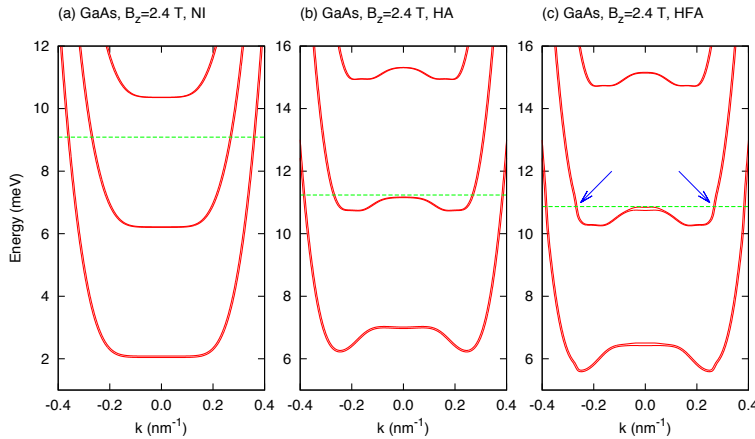


Figure 6.1: GaAs, energy spectra without Coulomb (or no interaction, NI), Hartree approximation (HA) and Hartree-Fock approximation (HFA), respectively. The arrows indicate enhanced energy dispersion created by the exchange effects.

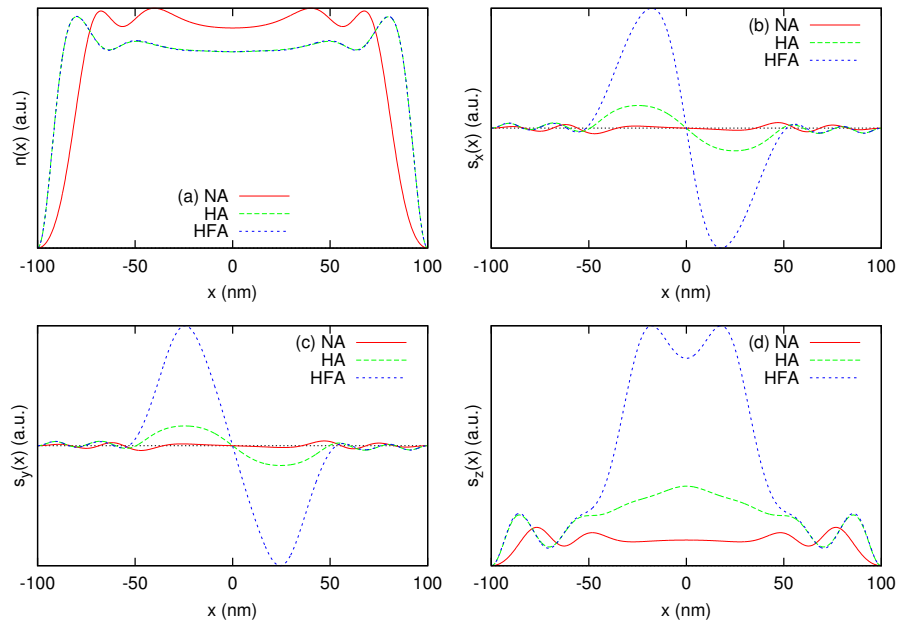


Figure 6.2: Charge densities GaAs $B=2.4$ T in arbitrary units. The thin horizontal line corresponds to zero density. The charge density is actually the electron density $n(x)$ which is positive. The spin density $s_z(x)$ is also positive.

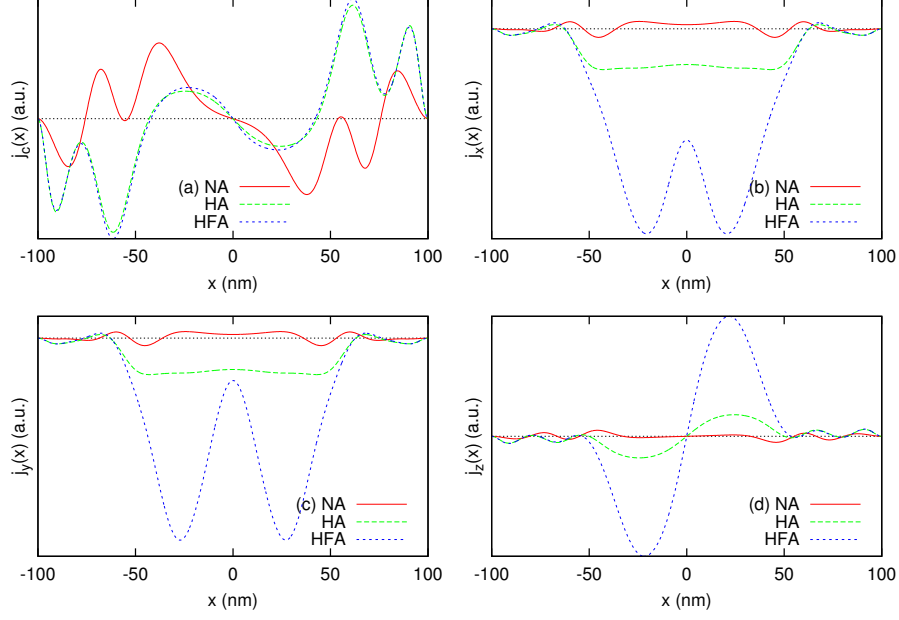


Figure 6.3: Current densities GaAs $B=2.4$ T. The thin horizontal line corresponds to zero current density.

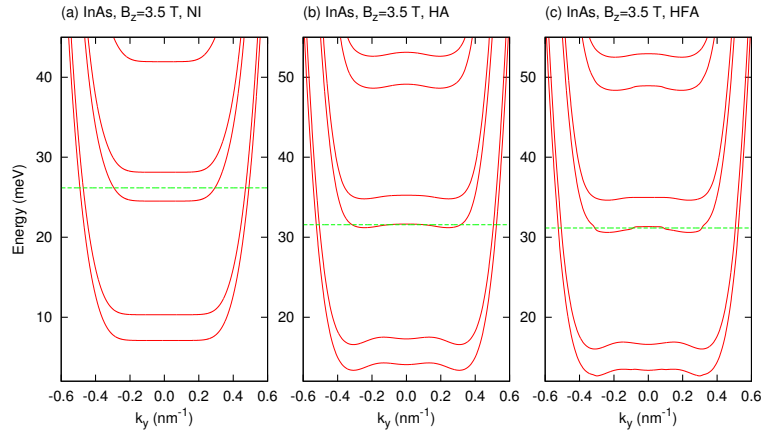


Figure 6.4: InAs, energy spectra without Coulomb, with Hartree and with Hartree-Fock respectively.

Chapter 7

Spin and Current Densities for Variable Magnetic Fields

7.1 Magnetic Field in z Direction and Symmetric Confinement

When the system is symmetric, looking at a cross section of the wire, one can think of an electron on each side of the system with the same height on the energy spectrum. When the external magnetic field is perpendicular to the wire, those two electrons move in the opposite direction. The electrons carry the same charge and opposite velocities, since the velocity is proportional to the slope of the energy functions in the spectrum.

$$\frac{\partial E_{nk}}{\partial k} = \frac{\hbar^2 k}{m} = \hbar \mathbf{v} .$$

This means that the charge current density is an odd function so the total charge current over the wire is zero. On the other hand spin currents can exist in a symmetric system. When observing the same example as before with one electron on each side of the spectrum they still have opposite velocities but if they have opposite spin x direction then a total spin current is induced[11]. This happens with the SOI, without SOI there would be no spin orientation and no spin currents as can be seen in chapter 5.

Now, when the external magnetic field is increased, the energy spectrum widens and the chemical potential decreases. When the chemical potential goes below a minimum in the energy spectrum the total spin current reaches an extremum and either increases or decreases. This happens because the spin orientation of the electrons changes. In Fig. 7.1 one can see the oscillations of the total spin x current in InAs with the magnetic field varying from

0 to 5 T. After about 4.5 T the oscillations stop since the chemical potential is between the two lowest energy bands. The Coulomb interaction is not included in these results.

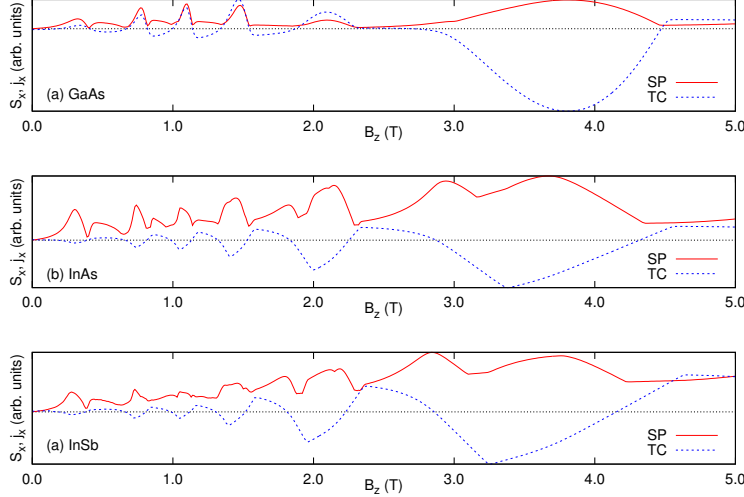


Figure 7.1: Spin x polarization amplitude (SP, continuous line) and total spin current (TC, dashed line) as functions of magnetic field B_z for noninteracting electrons, for the three materials considered: (a) GaAs, (b) InAs, (c) InSb. The thin horizontal dotted line shows the zero of the horizontal axis. The units are arbitrary and scaled to fit the curves on the same scale.

The Coulomb effects are shown in Figs. 7.2-7.7. The amplitude of the spin polarization is shown in all three directions x, y, z , and the total spin current for the x and y spin orientations. The total spin current z is zero, just like the total charge current. The results for GaAs, InAs and InSb, are shown separately and in each case the noninteracting (NI), the Hartree approximation (HA), and the Hartree-Fock approximation (HFA) are presented.

For GaAs the Hartree approximation yields oscillations of the spin polarization of about the same magnitude as for noninteracting electrons, Fig. 7.2. The oscillations are however denser with Coulomb interaction included. The reason is the widening of the charge density due to the Coulomb repulsion. The energy bands are separated by energy intervals roughly proportional to the inverse square of the width of the quantum wire. Due to the increased effective width of the quantum wire through Coulomb repulsion, the gaps between consecutive bands is reduced. Further, in the Hartree-Fock approximation, as expected, for GaAs the oscillations of the spin polarization amplitude and of the spin currents are enhanced by the exchange, progressively

with increasing the magnetic field, up to about three times or more. Since the in-plane spin densities (x and y) are determined by the SOI, one can again say that the SOI strengths are renormalized by the Coulomb effects, an effect which increases with the magnetic field strength. In the present study it was not possible to go beyond $B_z > 3$ T due to convergence problems or instability of the Hartree-Fock equations.

In Fig. 7.3(a)-(b) the total spin currents with polarization in the x and y directions, are shown respectively. A slight increase of the oscillation amplitude already in the Hartree approximation should be noted. The peak of the current at $B_z \approx 1.8$ T is obtained with the Fermi level at the bottom of the third band and has to be compared with the analog situation without interaction which occurs at $B_z \approx 2.1$ T. The previous peaks on the B_z scale correspond to the Fermi energy situated at the bottom of the fourth band. This enhancement effect can be interpreted as a result of the charge redistribution on the energy spectrum. In Fig. 7.3(b), together with the resulting energy "pockets", the slope of the energy dispersion at the Fermi level increases (and further increases in HFA). Therefore the velocity becomes slightly higher even in HA, and thus the spin currents may increase.

In Fig. 7.2 the spin polarization amplitude is increased with the Coulomb interaction and especially the exchange term. It can also be seen in Fig. 7.3 that the total currents for GaAs increase with the Hartree-Fock approximation.

In Figs. 7.4- 7.7 it's clear that the Coulomb interaction has less effect in InAs and InSb. The g -factor is larger for those materials than for GaAs so the effects of widening the wire in k -space by including the Coulomb interaction is not as noticeable.

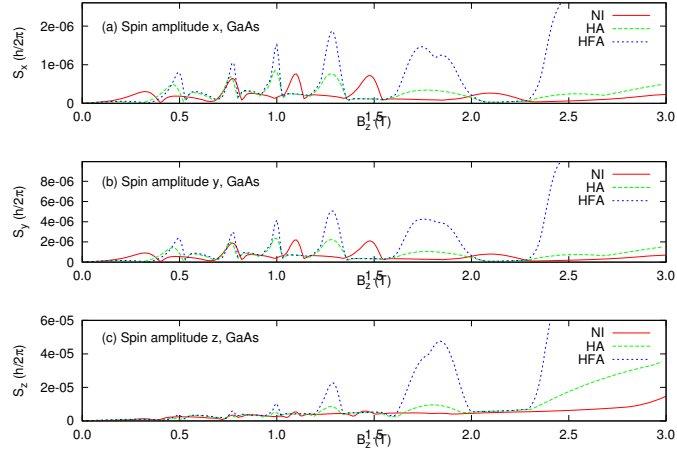


Figure 7.2: Magnetic field in z direction, spin polarization for GaAs.

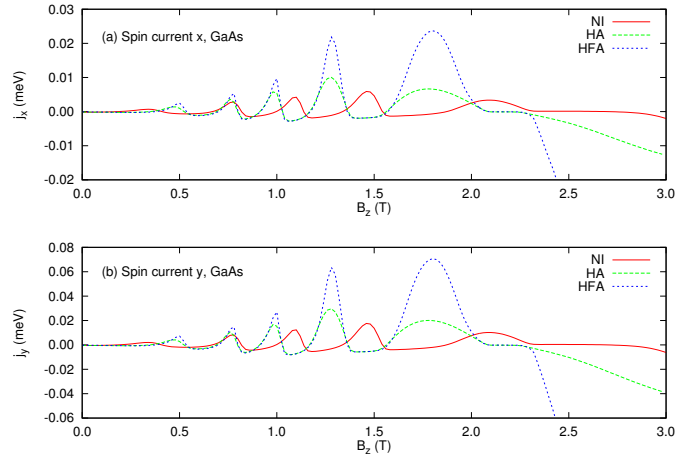


Figure 7.3: Magnetic field in z direction, total current for GaAs.

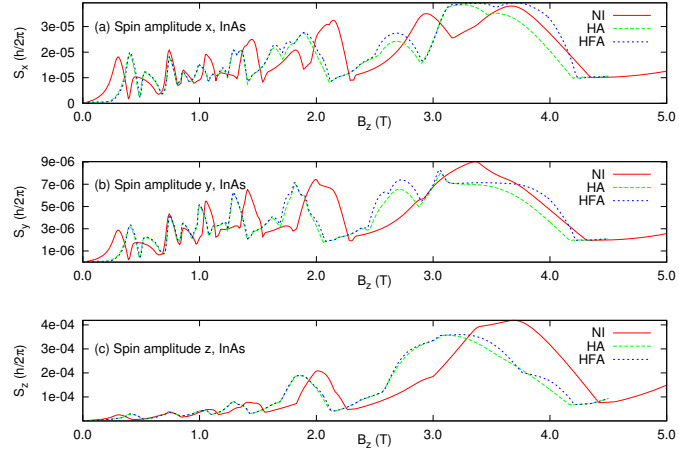


Figure 7.4: Magnetic field in z direction, spin polarization for InAs.

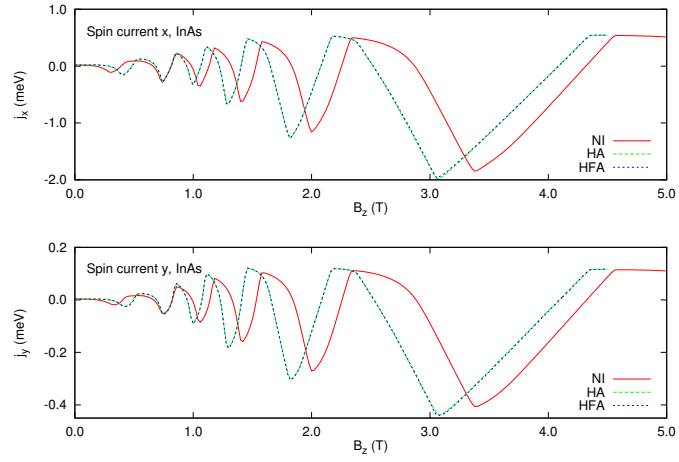


Figure 7.5: Magnetic field in z direction, total current for InAs.

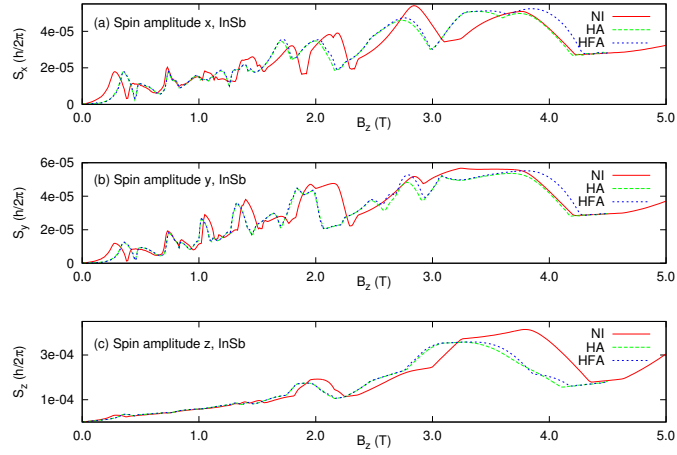


Figure 7.6: Magnetic field in z direction, spin polarization for InSb.

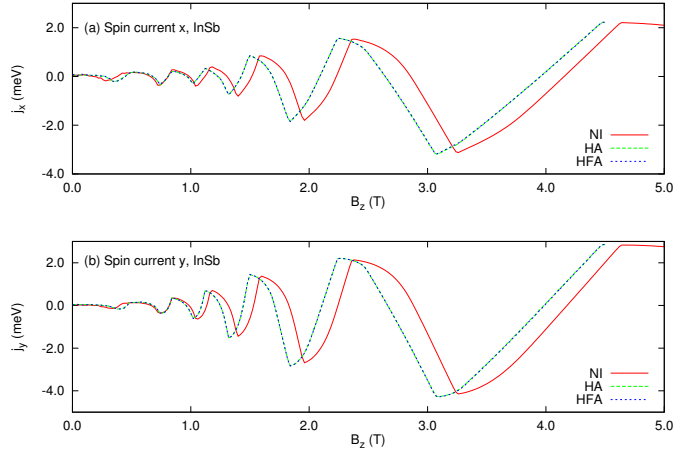


Figure 7.7: Magnetic field in z direction, total current for InSb.

7.2 Magnetic Field in z Direction and Asymmetric Confinement

Now the quantum wire with an asymmetric confinement is considered. To do that a potential bias of $V = 40$ mV is assumed in the direction x . Thus a triangular asymmetric quantum wire as shown in Fig. 2.2 is considered. The confinement can either be created during the growth process, or it may possibly be controlled by a variable external electric field in the x direction produced with metallic gates. In Figs. 7.8 and 7.9 examples of energy spectra for GaAs and InAs are shown in the three approximations studied. In this case the relatively smooth dispersion of the electrostatic potential across the wire leads to the relatively flat regions in the energy spectrum in the k space, for $k \approx 0.1$ in GaAs, and $k \approx -0.2$ in InAs, in the hartree approximation (Figs. 7.8(b) and 7.9(b) respectively). The exchange interaction introduces a step at these points, and opens the spin gap in GaAs, but as before, it has only a small effect in InAs ((Figs. 7.8(c) and 7.9(c)).

As can be seen in Figs. 7.8 and 7.9 the spectrum widens in k space with the Coulomb interaction. This is due to the repulsive nature of the Coulomb. In Figs. 7.10 to 7.15 both the spin polarization and total current can be seen for GaAs, InAs and InSb for a varying magnetic field. The enhancement of the amplitudes is still largest by far for the GaAs strip and especially with the exchange part. This is because the exchange interaction increases the dispersion and thus the velocity and the currents. But as can be seen in Figs. 7.8 and 7.9 the InAs spectrum widens with the direct interaction but does not change much by adding the exchange part. The GaAs however shows big change in spectra by adding the exchange part to the Coulomb interactions since the band gaps of GaAs are small compared to InAs and InSb which gives the exchange interaction relatively more effect.

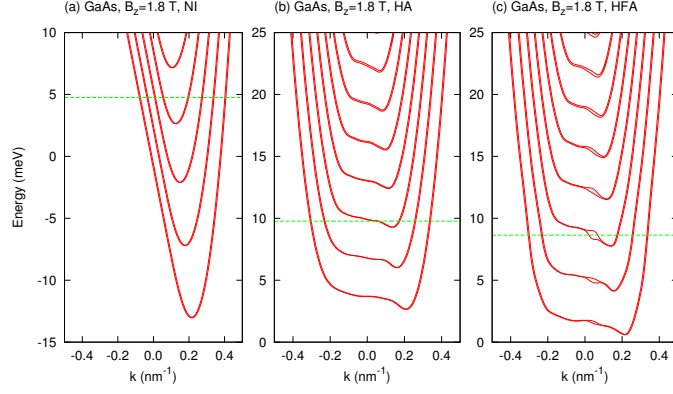


Figure 7.8: GaAs, asymmetric wire, energy spectra without Coulomb (NI), with Hartree (HA), and with Hartree-Fock (HFA) respectively.

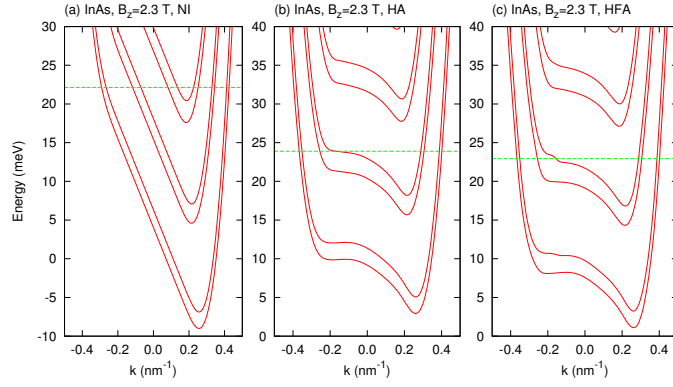


Figure 7.9: InAs, asymmetric wire, energy spectra without Coulomb (NI), with Hartree (HA), and with Hartree-Fock (HFA) respectively.

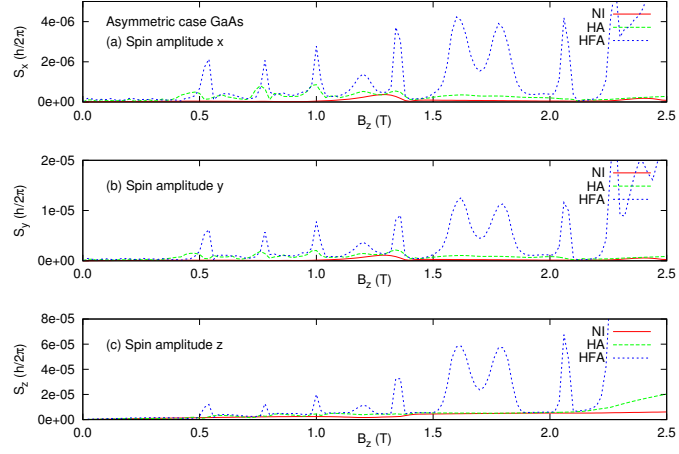


Figure 7.10: Asymmetric magnetic field in z direction, spin polarization for GaAs.

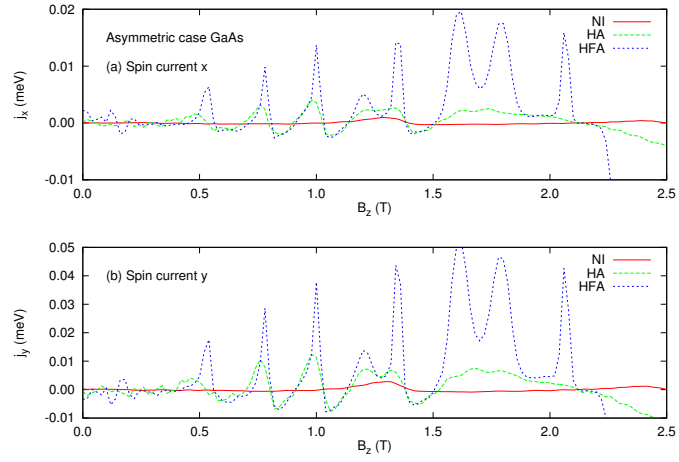


Figure 7.11: Asymmetric magnetic field in z direction, total current for GaAs.

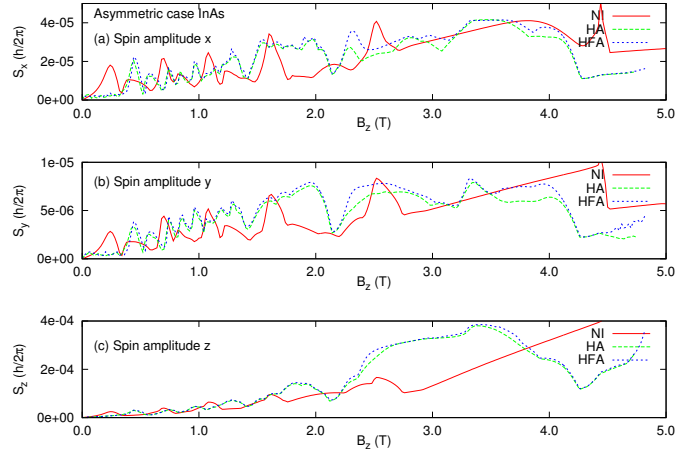


Figure 7.12: Asymmetric magnetic field in z direction, spin polarization for InAs.

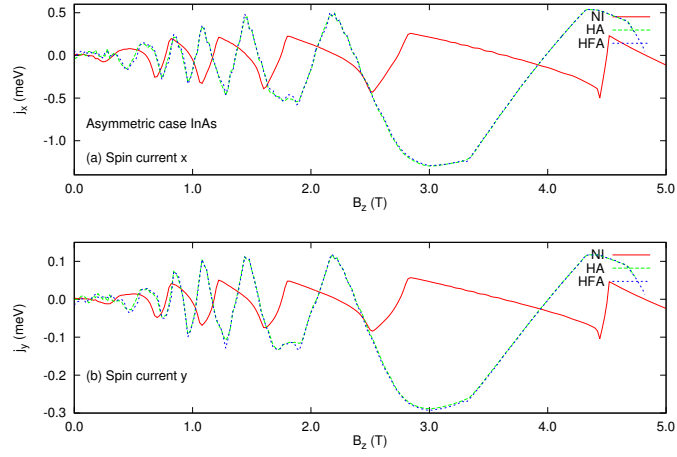


Figure 7.13: Asymmetric magnetic field in z direction, total current for InAs.

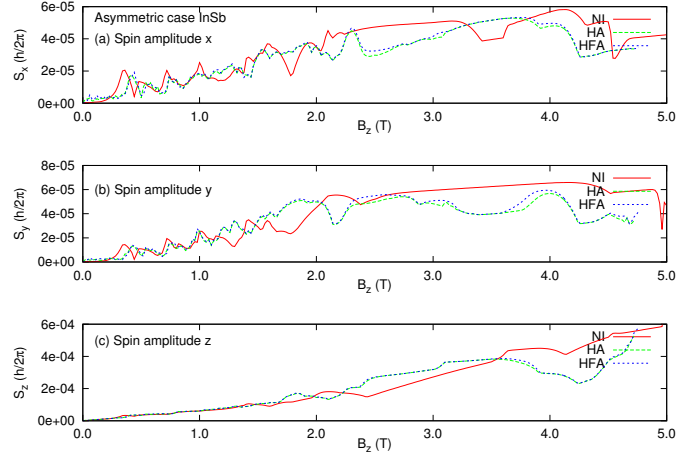


Figure 7.14: Asymmetric magnetic field in z direction, spin polarization for InSb.

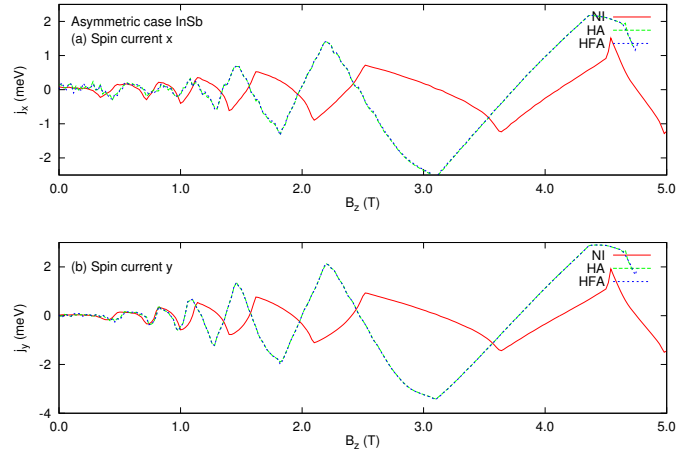


Figure 7.15: Asymmetric magnetic field in z direction, total current for InSb.

7.3 Magnetic Field in y Direction

In this section the amplitude of the spin polarization and the net spin currents for variable in-plane field along the quantum wire is discussed. One can see both of them in Fig. 7.16 for non-interacting electrons, for the three materials considered. This is the analog of Fig. 7.1. Now the oscillations occur over much larger intervals of the magnetic field for InAs and InSb, but no oscillation is seen for GaAs. To understand these results we look at the energy spectrum for InSb shown in Fig. 7.17(a), which is calculated for $B_y = 2$ T. At this magnetic field the spin amplitude and currents for InSb have a maximum and a minimum, respectively, in Fig. 7.16 (c). The chemical potential is situated at the bottom of the energy band 14, counted in the increasing energy order. At a lower magnetic field, for example at $B_y = 1$ T, the chemical potential is slightly higher, so an even number of energy bands are occupied (not shown). Obviously each band has a different occupation fraction, but the configuration corresponds to compensated spin chirality at least for $k = 0$. At a higher magnetic field, for example $B_y = 3$ T, the spin gaps further increase and the chemical potential drops slightly below the bottom of band 14 (also not shown), such that only 13 bands are now occupied and we obtain uncompensated spin chiralities around the center of the energy bands. Therefore at $B = 2$ T we have a smooth change of the spin polarization, and implicitly of the currents. Larger magnetic fields are needed to see the same maximum/minimum for InAs, which have a smaller spin gap, Fig. 7.16 (b), and probably a lot larger for GaAs, where we only see the initial increase of the polarization and only a very weak current, Fig. 7.16 (a).

Finally, in the next three figures, Figs. 7.18, 7.19, and 7.20, we show the effect of the Coulomb interaction on the spin polarization and spin currents. Again, to understand the results we begin with the InSb material. In Fig. 7.17(b) the Hartree approximation of the energy spectrum is shown, as before, for $B = 2$ T. The chemical potential is slightly above the bottom of band 14, almost like for a lower band in the non-interacting case. The reason is again the inflation of the charge distribution in the x direction, due to the Coulomb repulsion. The consequence is the reduction of the energy gaps corresponding to the lateral quantization and thus a relative shift upwards of the chemical potential. Therefore the minima or maxima of the spin currents shift to higher fields. As before, the Hartree and Hartree-Fock approximations give practically identical results for InAs and InSb. For GaAs however we can identify again the more pronounced exchange enhancement as before, although the spin currents for this material are orders of magnitude smaller than for the other two.

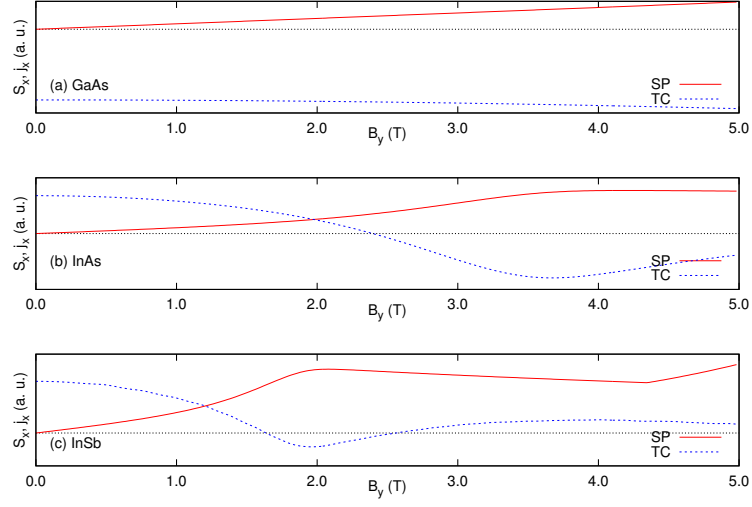


Figure 7.16: Spin x polarization amplitude (SP, continuous line) and total spin current (TC, dashed line) as functions of magnetic field B_y for noninteracting electrons, for the three materials considered: (a) GaAs, (b) InAs, (c) InSb. The thin horizontal dotted line shows the zero of the horizontal axis. The units are arbitrary and scaled to fit the curves on the same scale.

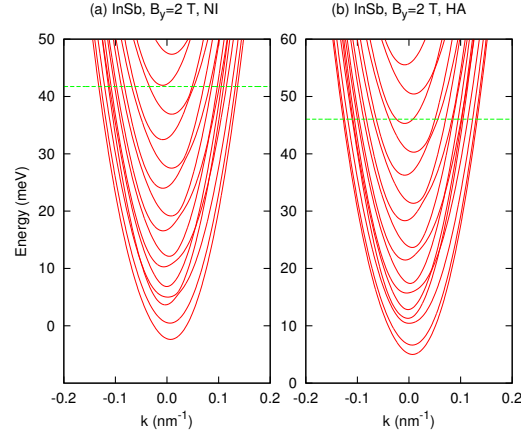


Figure 7.17: The energy spectra of InSb (a) without Coulomb and (b) in the Hartree approximation.

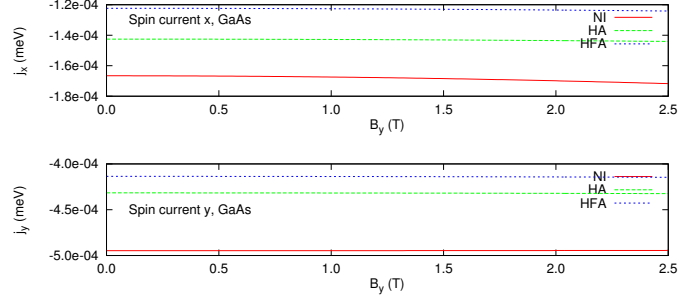


Figure 7.18: Magnetic field in y direction, total current for GaAs.

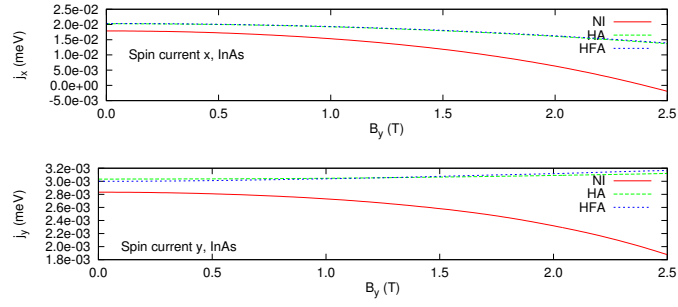


Figure 7.19: Magnetic field in y direction, total current for InAs.

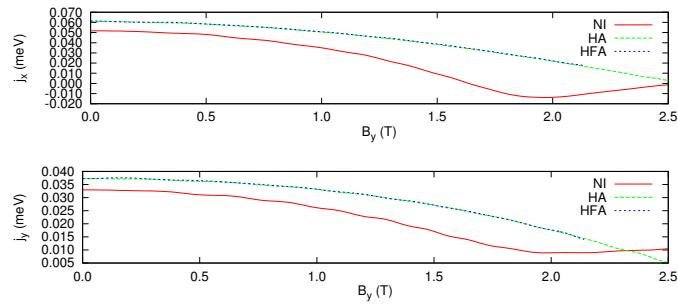


Figure 7.20: Magnetic field in y direction, total current for InSb.

Chapter 8

Summary and Conclusions

Coulomb interactions affect the energy spectrum, charge density, spin polarization and spin currents of a quantum wire. The size of these effects depends on a few properties. Firstly the material the wire is made of. Three materials were studied and the Coulomb interactions had most effects on GaAs, especially the exchange part of the Coulomb effects. The spin gap of GaAs is much smaller than of InAs and InSb if the Coulomb interaction is neglected. The exchange part of the Coulomb interaction amplifies the spin gap of GaAs possibly making GaAs comparable to the other materials. The exchange interaction has much smaller effects on the spin gap of InAs and InSb.

External magnetic field is also a factor, both the direction of the magnetic field and the strength. When the external magnetic field is perpendicular to the wire, and the wire has a symmetric confinement, the amplitude of the spin polarization oscillates with increasing magnetic field. This happens because increasing magnetic field lowers the chemical potential and when the chemical potential goes below the minimum of an energy band the spin orientation of the electrons changes and the spin polarization reaches an extrema. In this case there are also oscillating spin x and spin y currents since electrons traveling on the same velocity with opposite spin orientations will produce spin currents along the length of the wire. The amplitude of the oscillations are strongly affected by Coulomb interactions for GaAs and less, but still considerable for both InAs and InSb. For InAs and InSb the spin currents may be amplified by the direct Coulomb interaction via the redistribution of charge across the wire and the self consistent energy spectrum. The amplification of the spin currents can further increase in the presence of an in-plane electric field which corresponds to an asymmetric confinement.

A magnetic field along the wire produces different effects. Oscillations of the spin currents occur over larger intervals of the magnetic field for all

materials because the chemical potential varies slowly with a change in the magnetic field. Coulomb interactions may also affect the spin currents in this case through the same mechanism related to the charge distribution and energy spectrum.

Appendix A

Clarification of some Calculations

A.1 Function to calculate matrix elements of magnetic part

$$\begin{aligned}(x^m)_{nn'} &= \langle n | x^m | n' \rangle = \int_{-d}^d dx \varphi_n(x) x^m \varphi_{n'}(x) \\ &= \frac{2}{L_x} \int_{-L_x/2}^{L_x/2} dx x^m \sin \frac{n(x + \frac{1}{2}L_x)\pi}{L_x} \sin \frac{n'(x + \frac{1}{2}L_x)\pi}{L_x} = L_x^m I2s\left(m; -\frac{\pi}{2}; n, n'\right) ,\end{aligned}$$

where

$$\begin{aligned}I2s(m; c; n, n') &= \frac{2}{\Gamma_1^{m+1}} \int_0^\pi dt (t+c)^m \sin nt \sin n't \\ &= \frac{1}{\Gamma_1^{m+1}} [\text{Icos}(m; c; n - n') - \text{Icos}(m; c; n + n')] ,\end{aligned}$$

where

$$\text{Icos}(m; c; n) = \int_0^\pi dt (t+c)^m \cos nt ,$$

with $m = 0, 1, 2$. Now

$$\begin{aligned} \text{Icos}(0; c, n) &= \frac{(-1)^n}{n} \\ \text{Icos}(1, c, n) &= \frac{(-1)^n - 1}{n^2} \\ \text{Icos}(2; c, n) &= \frac{-2c + 2(c + \pi)(-1)^n}{n^2} . \end{aligned}$$

A.2 Orbital Contribution to Current Densities

$$v_y^{\text{orb}} = \frac{1}{i\hbar} \left[y, \frac{(p_y + eBx)^2}{2m} \right] = \frac{1}{m} (p_y + eBx) = \frac{1}{m} (-i\hbar\partial_y + eBx) ,$$

where

$$-i\hbar\partial_y\varphi_{ak}(\mathbf{r}) = \hbar k\psi_{ak}(\mathbf{r}) .$$

$$\langle \mathbf{J}_\mu^{\text{orb}}(x) \rangle = \frac{\hbar}{2} \sum_{ak} \mathcal{F}_{ak} \left(\Re \sum_{\sigma_1\sigma_2} \psi_{ak}^*(x, \sigma_1) (\mathbf{J}_\mu)_{\sigma_1\sigma_2} \psi_{ak}(x, \sigma_2) \right) \frac{\hbar k + eBx}{m} \frac{1}{L_y}$$

$$\psi_{ak}(x, \sigma) = \sum_n c_a(nk\sigma) \varphi_n(x)$$

$$\langle \mathbf{J}_\mu^{\text{orb}}(x) \rangle = \frac{\hbar}{2} \sum_{nn'} \varphi_n(x) \varphi_{n'}(x) \Re \left(\sum_{\sigma_1\sigma_2} \frac{1}{L_y} \sum_{ak} \mathcal{F}_{ak} c_a^*(nk\sigma') c_a(n'k\sigma) (\sigma_\mu)_{\sigma_1\sigma_2} \frac{\hbar k + eBx}{m} \right)$$

$$\frac{1}{L_y} \sum_{ak} \mathcal{F}_{ak} c_a^*(nk\sigma) c_a(n'k\sigma') = \frac{1}{2\pi} \int dk \mathcal{F}_{ak} c_a^*(nk\sigma) c_a(n'k\sigma') = \text{Gmat}(q, q') ,$$

with $q = (n\sigma)$ and $q' = (n'\sigma')$.

$$\begin{aligned} \langle \mathbf{J}_\mu^{\text{orb}}(x) \rangle &= \frac{\hbar}{2} \sum_{qq'} \varphi_q(x) \varphi_{q'}(x) \Re \left[\text{Gmat}(q, q') \frac{\hbar}{m} + \text{Gmat}(q, q') \frac{eBx}{m} \right] (\sigma_\mu)_{\sigma\sigma'} \\ &= \frac{\hbar}{2} \frac{\hbar}{m} \sum_{qq'} \varphi_q(x) \varphi_{q'}(x) \Re \left[\text{Gmat}(q, q') + \text{Gmat}(q, q') \frac{x}{l_B^2} \right] (\sigma_\mu)_{\sigma\sigma'} . \end{aligned}$$

Now, if $\mu = 0$ then $(\sigma_\mu)_{\sigma\sigma'} = \frac{2}{\hbar} e \delta_{\sigma\sigma'}$ with prefactor $\frac{e\hbar}{m}$ and for $\mu = x, y, z$ the prefactor is $\frac{\hbar^2}{2m}$.

A.3 SOI Contribution to Current Densities

$$v_y^{\text{soi}} = \frac{1}{i\hbar} [y, H_{\text{soi}}] = \frac{1}{i\hbar} \left[y, \frac{\alpha}{\hbar} (\sigma_x p_y - \sigma_y p_x) + \frac{\beta}{\hbar} (\sigma_y p_y - \sigma_x p_x) \right] ,$$

with $[y, p_y] = i\hbar$ and so

$$v_y^{\text{soi}} = \frac{\alpha}{\hbar} \sigma_x - \frac{\beta}{\hbar} \sigma_y ,$$

and

$$\langle \mathbf{J}_\mu^{\text{soi}}(x) \rangle = \frac{\hbar}{2} \sum_{ak} \mathcal{F}_{ak} \Re \sum_{\sigma_1 \sigma_2} \psi_{ak}^*(x, \sigma_1) \left(\frac{\alpha}{\hbar} \sigma_\mu \sigma_x - \frac{\beta}{\hbar} \sigma_\mu \sigma_y \right)_{\sigma_1 \sigma_2} \psi_{ak}(x, \sigma_2) \frac{1}{L_y} ,$$

and for $\mu = 0, x, y, z$ the relations hold

$$\sigma_x \sigma_y = i\sigma_z, \quad \sigma_y \sigma_z = i\sigma_x, \quad \sigma_z \sigma_x = i\sigma_y$$

$$\sigma_i \sigma_j + \sigma_j \sigma_i = 2\delta_{ij}$$

$$\sigma_x^2 = \sigma_y^2 = \sigma_z^2 = 1 .$$

Using these relations the different currents are

$$\langle \mathbf{J}_\mu^{\text{soi}}(x) \rangle = \frac{\hbar}{2} \frac{1}{L_y} \sum_{ak} \mathcal{F}_{ak} \Re \sum_{\sigma_1 \sigma_2} \psi_{ak}^*(x, \sigma_1) \psi_{ak}(x, \sigma_2) \cdot \underbrace{\begin{cases} \frac{2e}{\hbar} \left(\frac{\alpha}{\hbar} \sigma_x - \frac{\beta}{\hbar} \sigma_y \right)_{\sigma_1 \sigma_2} & , \mu = 0 \\ \frac{\alpha}{\hbar} \delta_{\sigma_1 \sigma_2} & , \mu = x \\ -\frac{\beta}{\hbar} \delta_{\sigma_1 \sigma_2} & , \mu = y \\ 0 & , \mu = z \end{cases}}_{\lambda_{\sigma\sigma'}} ,$$

so

$$\langle \mathbf{J}_\mu^{\text{soi}}(x) \rangle = \frac{\hbar}{2} \sum_{qq'} \varphi_n(x) \varphi_{n'}(x) \Re [\text{Gmat}(q, q') \lambda_{\sigma\sigma'}] .$$

A.4 Exchange Contribution to Current Densities

$$v_y^{\text{ex}} = \frac{1}{i\hbar} [y, \Sigma_F] ,$$

where the self energy Σ_F is a complex operator.

$$(\Sigma_F \varphi)(\mathbf{r}) = \int d\mathbf{r}' \Sigma_F(\mathbf{r}, \mathbf{r}') \varphi(\mathbf{r}'), \quad \forall \varphi \in \text{Hilbert space}$$

$$([\mathbf{r}, \Sigma_F] \varphi)(\mathbf{r}) = \int d\mathbf{r}' \mathbf{r} \Sigma_F(\mathbf{r}, \mathbf{r}') \varphi(\mathbf{r}') - \int d\mathbf{r}' \Sigma_F(\mathbf{r}, \mathbf{r}') \mathbf{r}' \varphi(\mathbf{r}') = \int d\mathbf{r}' (\mathbf{r} - \mathbf{r}') \Sigma_F(\mathbf{r}, \mathbf{r}') \varphi(\mathbf{r}')$$

$$\begin{aligned}
\Sigma_F(\mathbf{r}, \mathbf{r}') &= -u(\mathbf{r} - \mathbf{r}') \sum_{ak} \mathcal{F}_{ak} \psi_{ak}(\mathbf{r}) \psi_{ak}^\dagger(\mathbf{r}') \\
\langle \mathbf{J}_\mu^{ex}(x) \rangle &= \frac{\hbar}{2} \sum_{ak} \mathcal{F}_{ak} \Re \sum_{\sigma_1 \sigma_2} \psi_{ak}^\dagger(\mathbf{r}, \sigma_1) \left(\sigma_\mu \frac{1}{i\hbar} [y, \Sigma_F] \right)_{\sigma_1 \sigma_2} \psi_{ak}(\mathbf{r}, \sigma_2) \\
&= [y, \Sigma_F]_{\sigma_1 \sigma_2} \psi_{ak}(\mathbf{r}', \sigma_3) \\
&= \int d\mathbf{r}' (y - y') (\Sigma_F(\mathbf{r}, \mathbf{r}'))_{\sigma_1 \sigma_2} \psi_{ak}(\mathbf{r}', \sigma_3) \\
&= \int d\mathbf{r}' (y - y') \left[-u(\mathbf{r} - \mathbf{r}') \sum_{a'k'} \mathcal{F}_{a'k'} \psi_{a'k'}(\mathbf{r}, \sigma_1) \psi_{a'k'}^\dagger(\mathbf{r}', \sigma_2) \right] \psi_{ak}(\mathbf{r}', \sigma_3) \\
&= - \sum_{a'k'} \mathcal{F}_{a'k'} \psi_{a'k'}(\mathbf{r}', \sigma_1) \int d\mathbf{r}' (y - y') u(\mathbf{r} - \mathbf{r}') \psi_{a'k'}^*(\mathbf{r}, \sigma_2) \psi_{ak}(\mathbf{r}', \sigma_3) \\
&= - \frac{e^2}{\kappa L_y^{3/2}} \sum_{a'k'} \mathcal{F}_{a'k'} \psi_{a'k'}(x, \sigma_1) e^{ik'y} \int dx' dy' \frac{y - y'}{\sqrt{(x - x')^2 + (y - y')^2}} \\
&\quad \cdot \psi_{a'k'}^*(x', \sigma_2) e^{-ik'y'} \psi_{ak}(x', \sigma_3) e^{iky'} \\
&= \frac{e^2}{\kappa L_y^{3/2}} \sum_{a'k'} \mathcal{F}_{a'k'} \psi_{a'k'}(x, \sigma_1) e^{iky} \int dx' dz \frac{z e^{i(k-k')z}}{\sqrt{(x - x')^2 + z^2}} \psi_{a'k'}^*(x', \sigma_2) \psi_{ak}(x', \sigma_3) ,
\end{aligned}$$

where $y - y' = z$, $y' = y - z$ and $dy' = -dz$. Now

$$\begin{aligned}
\int dz \frac{z e^{i(k-k')z}}{\sqrt{(x - x')^2 + z^2}} &= 2i \int_0^\infty dz \frac{z \sin |k - k'|z}{\sqrt{(x - x')^2 + z^2}} \text{sign}(k' - k) \\
\int_0^\infty \frac{\cos ax \, dx}{\sqrt{\beta^2 + x^2}} &= K_0(a\beta), \quad a > 0, \beta > 0 \\
\frac{d}{da} &\Rightarrow - \int_0^\infty \frac{x \sin ax \, dx}{\sqrt{\beta^2 + x^2}} = K'_0(a\beta)\beta = -K_1(a\beta)\beta \\
&\Rightarrow \int_0^\infty dz \frac{z \sin(|k' - k|z)}{\sqrt{(x - x')^2 + z^2}} = |x' - x| K_1(|(k - k')(x - x')|) .
\end{aligned}$$

Now

$$\begin{aligned}
[y, \Sigma_F]_{\sigma_1 \sigma_2} \psi_{ak}(\mathbf{r}, \sigma_3) &= \frac{e^2}{\kappa L_y^{3/2}} (2i) e^{iky} \sum_{a'k'} \mathcal{F}_{a'k'} \text{sign}(k - k') \psi_{a'k'}(x, \sigma_1) \cdot \\
&\quad \cdot \int dx' |x - x'| K_1(|(k' - k)(x' - x)|) \psi_{a'k'}^*(x', \sigma_2) \psi_{ak}(x', \sigma_3) ,
\end{aligned}$$

which gives the current density

$$\begin{aligned}
\langle \mathbf{J}_\mu^{ex}(x) \rangle &= \frac{\hbar}{2} \frac{e^2}{\kappa L_y^2} (2i) \frac{1}{i\hbar} \sum_{ak} \mathcal{F}_{ak} \Re \sum_{\substack{\sigma_1 \sigma_2 \\ \sigma'}} \psi_{ak}^*(x, \sigma') \text{sign}(k' - k) \cdot \\
&\quad \cdot \int dx' |x' - x| K_1(|k' - k| |x' - x|) \sum_{\sigma_2} \psi_{a'k'}^*(x', \sigma_2) \psi_{ak}(x', \sigma_2) \\
&= \frac{e^2}{\kappa L_y^2} \Re \sum_{\substack{ak \\ a'k'}} \left[\mathcal{F}_{ak} \mathcal{F}_{a'k'} \sum_{\sigma_1 \sigma'} \psi_{ak}^*(x, \sigma_1) (\sigma_\mu)_{\sigma_1 \sigma'} \psi_{a'k'}(x, \sigma') \cdot \right. \\
&\quad \left. \cdot \text{sign}(k' - k) \int dx' |x' - x| K_1(|k' - k| |x' - x|) \sum_{\sigma_2} \psi_{a'k'}^*(x', \sigma_2) \psi_{ak}(x', \sigma_2) \right] .
\end{aligned}$$

Now observe that if

$$A = \sum_{\substack{ak \\ a'k'}} [\dots] ,$$

and

$$A^* = \sum_{\substack{ak \\ a'k'}} [\dots]^* = -A ,$$

since $\text{sign}(k - k') = -\text{sign}(k' - k)$, that

$$\Re A = \frac{1}{2} (A + A^*) = 0 ,$$

that is

$$\langle \mathbf{J}_\mu^{ex}(x) \rangle = 0, \quad \forall y .$$

A.5 Prefactors and Units for Current Densities

The charge current has $\mu = 0$ so

$$\begin{aligned}
\langle \mathbf{J}_0(x) \rangle &= \langle \mathbf{J}_o^{\text{rob}} + \mathbf{J}_0^{\text{soi}}(x) \rangle \\
&= e \sum_{qq'} \varphi_n(x) \varphi_{n'}(x) \Re \left\{ \text{Gmat} k(q, q') \frac{\hbar}{m} \delta_{\sigma\sigma'} \right. \\
&\quad \left. + \text{Gmat}(q, q') \left[\frac{eBx}{m} \delta_{\sigma\sigma'} + \frac{\alpha}{\hbar} (\sigma_x)_{\sigma\sigma'} - \frac{\beta}{\hbar} (\sigma_y)_{\sigma\sigma'} \right] \right\} .
\end{aligned}$$

Here $\varphi_n(x)\varphi_{n'}(x) \sim \frac{1}{L(nm)}$, $\text{Gmat}k\frac{\hbar}{m} \sim \frac{1}{L^2(nm)}$, $\text{Gmat} \sim \frac{1}{L(nm)}$ and $\frac{eBx}{m} = \frac{\hbar}{m} \frac{x}{l_B^2} \sim \frac{\hbar}{m} \frac{1}{L(nm)}$. The units are

$$\mathbf{J}_0 : \frac{e}{L(nm)T(ns)}, \quad \text{units}\{\dots\} : \frac{1}{T(s)} = \frac{1}{T(ns) \cdot 10^9}$$

$$\frac{1}{L^2(nm)} \frac{\hbar}{m} = \frac{1}{L^2(nm)} \frac{ML^2T^{-1}}{M} = \frac{1}{10^{-18}} \frac{1}{T} = \frac{10^{18}}{T(s)} \Rightarrow \frac{\hbar}{m} \rightarrow c_1 = \frac{10^{18}\hbar}{m} \frac{1}{10^9} (ns)$$

$$\frac{\alpha(meVnm)}{\hbar} = \frac{\alpha \cdot 10^{-3} \cdot e(ynm)}{\hbar} \cdot \frac{1}{10^9} (ns)^{-1} = \alpha \cdot c_2$$

$$\langle \mathbf{J}_0(x) \rangle = e \sum_{qq'} \varphi_n(x) \varphi_{n'}(x) \Re \left\{ \text{Gmat}k(q, q') c_1 \delta_{\sigma\sigma'} \right. \\ \left. + \text{Gmat}(q, q') \left[c_1 \delta_{\sigma\sigma'} + c_2 (\alpha \sigma_x)_{\sigma\sigma'} - \beta (\sigma_y)_{\sigma\sigma'} \right] \right\},$$

with x, L_x and l_B in nm and α, β in $meVnm$.

For the spin current $\mu = x, y, z$ so

$$\langle \mathbf{J}_0(x) \rangle = \frac{\hbar}{2} \sum_{qq'} \varphi_n(x) \varphi_{n'}(x) \Re \left\{ \text{Gmat}k(q, q') c_1 (\sigma_\mu)_{\sigma\sigma'} \right. \\ \left. + \text{Gmat}(q, q') \left[c_1 (\sigma_\mu)_{\sigma\sigma'} + c_2 (\lambda_\mu)_{\sigma_1\sigma_2} \right] \right\},$$

where

$$(\lambda_\mu)_{\sigma_1\sigma_2} = \begin{cases} \alpha \delta_{\sigma_1\sigma_2} & , \mu = x \\ -\beta \delta_{\sigma_1\sigma_2} & , \mu = y \\ 0 & , \mu = z \end{cases},$$

with the units

$$\mathbf{J}_\mu = \frac{\hbar}{L(nm)T(ns)}.$$

Bibliography

- [1] Vidar Gudmundsson, Rolf R. Gerhardt, Robert Johnston and Ludwig Schweitzer, Z. Phys. B70, 453, 1988. 24
- [2] Ulrich Wulf, Vidar Gudmundsson and Rolf R. Gerhardt, Phys. Rev. B **38**, 4218, 1988. 24
- [3] Vidar Gudmundsson, *Screening of impurities in the quantum Hall regime, Spectroscopy of Semiconductor Microstructures*, NATO ASI Series B206, 517, Plenum Press, 1989. 24
- [4] Mack, Chris. Semiconductor Lithography (Photolithography) - The Basic Process. *Lithography*. 1 Aug. 2012. <<http://www.lithoguru.com/scientist/lithobasics.html>> 2
- [5] Ihn, Thomas. *Semiconductor Nanostructures*. Oxford: Oxford University Press, 2010. 1
- [6] S. Gujarathi, K. M. Alam and S. Pramanik. *Magnetic-field-induced spin texture in a quantum wire with linear Dresselhaus spin-orbit coupling*. Phys. Rev. B **85**, 045413, 2012.
- [7] S. Ihnatsenka and I. V. Zozoulenko. *Spin polarization of edge states and the magnetosubband structure in quantum wires*. Phys. Rev. B **73**, 075331, 2006. 21, 24
- [8] Sigurdur I. Erlingsson, J. Carlos Egues and Daniel Loss. Phys. Rev. B **82**, 155456 (2010).
- [9] M. Johnson and R. Silsbee. *Interfacial charge spin coupling: Injection and detection of spin magnetization in metals*. Phys. Rev. Lett. vol. **55**, p. 1790, 1985. 7
- [10] E. I. Rashba. *Spin-orbit coupling and spin transport*, arXiv cond-mat, vol. **0507007**v2:5, 2005. 8

- [11] S. Bandyopadhyay and M. Cahay. *Introduction to spintronics*. CRC Press, Boca Raton, 2008. 28
- [12] Y. A. Bychkov and I. E. Rashba. *Oscillatory effects and the magnetic susceptibility of carriers in inversion layers*, J. Phys. C, vol. **74**, p. 6039, 1984. 8
- [13] G. Dresselhaus. *Spin-orbit coupling effects in zinc blende structures* Phys. Rev. vol. **98**, p. 368, 1955. 8
- [14] J. Fabian, A. Matos-Abiaguea, C. Ertler, P. Stano and I. Zutic. *Semiconductor spintronics*. Bratislava: Slovak Academy of Sciences, 2002.
- [15] John Schliemann, J. Carlos Egues and Daniel Loss. *Nonballistic Spin-Field-Effect Transistor*. Phys. Rev. Lett. vol. **90** nr. 14, 2003.
- [16] Alexander L. Fetter and John Wilek Walecka. *Quantum Theory of Many Particle Systems*. Dover Publications, INC, Mineola, New York, 2003. 6, 10, 21
- [17] S. Doniach and E. H. Sondheimer. *Green's Functions for Solid State Physicists*. Imperial College Press, London, 2004.
- [18] Eugen Merzbacher. *Quantum Mechanics*. John Wiley & Sons, London, 1970. 21
- [19] B. Tanatar and D. M. Ceperley. *Ground state of the two-dimensional electron gas*. Phys. Rev. B, vol. **39**, nr. 8, 1989. 3
- [20] B. Tanatar, private communication. 21
- [21] Claudio Attaccalite, Saverio Moroni, Paola Gori-Giorgi and Giovanni B. Bachelet. *Correlation Energy and Spin Polarization in the 2D Electron Gas*. Phys. Rev. Lett. vol. **88**, nr. 25, 2002. 3
- [22] Andrei Manolescu and Rolf R. Gerhardts. *Exchange-enhanced spin splitting in a two-dimensional electron system with lateral modulation*. Phys. Rev. B, vol. **51**, nr. 3, 1995. 24
- [23] Andrei Manolescu and Rolf R. Gerhardts. *Coulomb effects on the quantum transport of a two-dimensional electron system in periodic electric and magnetic fields*. Phys. Rev. B, vol. **56**, nr. 15, 1997. 24
- [24] Claude Cohen-Tannoudji, Bernard Diu and Franck Laloe. *Quantum Mechanics*. Hermann and John Wiley & Sons, Singapore, 2005. 5, 15

- [25] *Nanolithography* Wikipedia: The Free Encyclopedia. Wikimedia Foundation, Inc. 22 July 2004. Web. 15 Aug. 2012.
- [26] *Spintronics*. Wikipedia: The Free Encyclopedia. Wikimedia Foundation, Inc. 22 July 2004. Web. 15 Aug. 2012.
- [27] *Vapor-liquid-solid method*. Wikipedia: The Free Encyclopedia. Wikimedia Foundation, Inc. 22 July 2004. Web. 15 Aug. 2012. 2
- [28] T. Ando and Y. Uemura, J. Phys. soc. Jpn. **37**, 1044 (1974).

2

24